[illegible]

[illegible]

High Energy Physics Division
Argonne National Laboratory
Argonne, Illinois [illegible]

ABSTRACT

A review is presented of [illegible] the [illegible] pair continuum [illegible] in [illegible] I begin with the [illegible] Drell-Yan quark [illegible] annihilation model [illegible] expectations are compared [illegible] Scaling [illegible] and corrections [illegible] the Drell-[illegible] are discussed [illegible] I present original work [illegible] understanding of the transverse momentum distri[illegible] dileptons. In a parton model, the quark-gluon sc[illegible] graphs which provide scaling violations also [illegible] leptons with relatively large p_T. Comparis[illegible] avail-able data support these QCD expectations; further tests of the QCD predictions are proposed. Implications are drawn for W-production experiments, and predictions are presented for reactions initiated by antiprotons.

*Invited paper to be published in the Proceedings of the 3rd International Conference at Vanderbilt University on New Results in High Energy Physics, March 6-8, 19[illegible]8.

TABLE OF CONTENTS

I. INTRODUCTION

My charge is to summarize our theoretical understanding of massive lepton-pair production in high energy collisions of hadrons:

$$h_1 + h_2 \to \ell^+\ell^- \text{ plus anything,}$$

where ℓ is an electron, muon, or heavy lepton (τ). The theory is evolving rapidly, in response, in part, to the ever increasing quality of the data.[1,2] Recently good tests have been made of several theoretical expectations, including the scaling hypothesis. A relatively new feature of the data is the observation that dileptons emerge with larger mean transverse momenta than previously supposed. The mean transverse momentum appears also to be independent of dilepton mass for $5 < M_{\mu\mu} < 10$ GeV. These $\langle p_T \rangle$ properties may be interpreted in a QCD framework in terms of the same types of quark-gluon diagrams which provide scaling violations.

In this report I focus for the most part on the dilepton continuum, the "background" above which one observes the resonances of the J/Ψ and Υ families. I begin with a short review of the traditional Drell-Yan annihilation model[3] and its experimental successes. Next I describe the reinterpretations of, or "corrections" to this model which are required in light of recent theoretical and experimental developments, including scaling violations in deep-inelastic electron and muon scattering. Finally, I report on some very recent work

which others and I have done in an attempt to interpret the transverse momentum distribution of lepton pairs.

There are various reasons for investigating the production of lepton pairs in hadronic reactions. The J/ψ and ϒ states were found this way, and it takes no imagination to suppose that the discovery of other new hadronic degrees of freedom (viz. heavier quarks) may be only a question of securing the greater acceptance, resolution, luminosity, and energy needed to probe even higher values of the dilepton mass. If there are new quarks, the $J^P = 1^-$ $Q\bar{Q}$ state will couple through a virtual photon to lepton pairs. Higgs mesons and the neutral vector boson mediator of weak interactions, the Z^0, should be observed as states in the $\ell^+\ell^-$ mass spectrum. Measurements of dilepton yields at present energies, along with the conserved vector current and scaling hypotheses, permit estimates to be made for charged weak vector boson $W^\pm$ yields at the much higher energies which should be available soon at CERN, Fermilab, and Brookhaven.

In this report, I concentrate on yet another aspect of the physics of massive lepton pair production in hadron collisions. The data provide a good opportunity to test various concepts regarding quarks and other partons, including:

a. Scaling and scaling violations.

b. The connection between $h_1h_2 \to \ell^+\ell^-X$ and the "crossed" processes, in which one or two leptons are in the initial state:

$$ep \rightarrow e'X \ ;$$

$$\mu p \rightarrow \mu'X \ ;$$

$$\nu p \rightarrow \mu X \ ;$$

$$e^+e^- \rightarrow \quad X \ .$$

c. QCD quark-gluon dynamical predictions for the p_T distribution of high mass lepton pairs (including the M, s and x_F dependences of $\langle p_T \rangle$).

d. The data also provide an independent determination of anti-quark and gluon momentum distributions. In the case of π induced reactions, e.g. $\pi N \rightarrow \mu\bar{\mu}X$, the quark structure functions for the pion may be deduced for the first time.

II. THE CLASSICAL DRELL-YAN ANNIHILATION MODEL

I eschew the usual warnings regarding the inapplicability of the "rigorous" operator product expansion to $h_1 h_2 \to \ell^+ \ell^- X$ and, instead, adopt the phenomenological Drell-Yan model[3] as a point of departure. In this model, it is supposed that when two hadrons collide, a quark constituent from one miraculously enough finds an antiquark constituent in the other hadron, with which it then annihilates through a single virtual photon of mass $M = \sqrt{Q^2}$. This process is sketched in Fig.1. The probability that a quark [antiquark] is present with longitudinal momentum fraction x of the parent hadron's momentum is expressed by a function $q(x)\left[\bar{q}(x)\right]$. In this classical Drell-Yan model the functions $q(x)$ and $\bar{q}(x)$ are independent of Q^2 — i.e. are scaling functions — and the quarks and antiquarks are assumed to carry neglible transverse momentum. Both assertions require modification, as I'll describe later. The longitudinal fractions x are positive, and $M^2 = Q^2 = s x_1 x_2$, where here x_1 refers to a quark (antiquark) from hadron 1, and x_2 labels an antiquark (quark) from hadron 2. It is supposed that $q(x)$ is a function derived from data on deep-inelastic electron and deep-inelastic muon scattering experiments, and that $\bar{q}(x)$ is likewise known as a result of studies of $\nu p \to \mu X$ and $\bar{\nu} p \to \mu X$. For large M^2, the oft-quoted Drell-Yan prediction for $h_1 h_2 \to \mu\bar{\mu} X$ or $h_1 h_2 \to e\bar{e} X$ is

$$M^4 \frac{d\sigma}{dM^2} = \frac{4\pi\alpha^2}{9} \sum_i e_i^2 \iint dx_1 dx_2 \left[q_i(x_1)\bar{q}_i(x_2) + \bar{q}_i(x_1) q_i(x_2) \right] \delta\left(x_1 x_2 - \frac{M^2}{s}\right). \quad (1)$$

The sum is taken over the different quark flavors, usually restricted for practical purposes to $i = u,d,$ and s. The factor 9 in the denominator is a product of two factors of 3, one derived from an angular integration in the final $\ell\bar{\ell}$ rest frame. The second is the famous "color factor"; e_i is the fractional quark charge. An integration may be "undone" easily in Eq. (1) to obtain expressions for $d\sigma/dM^2dy$ and $d\sigma/dM^2dx_F$, where y and x_F are the rapidity and scaled longitudinal momentum (Feynman x) of the lepton pair. I do not repeat those expressions here. For $h_1h_2 \to \tau^+\tau^-X$, the lepton mass ($m_\tau \sim 1.8$ GeV) is no longer negligible with respect to typical values of M, and a threshold factor

$$\left(1 - \frac{4m_\tau^2}{M^2}\right)^{\frac{1}{2}} \frac{3}{8}\left[\left(1 + \frac{4m_\tau^2}{M^2}\right) + \left(1 - \frac{4m_\tau^2}{M^2}\right)\cos^2\theta^*\right] \qquad (2)$$

must be inserted on the right hand side of Eq. (1). The τ is assumed to have spin 1/2. Displayed in Eq. (2) is the explicit angular dependence expected in the classical Drell-Yan model. In the $\tau^+\tau^-$ rest-frame, θ^* is the polar angle of a τ with respect to the axis defined by the collinear $q\bar{q}$ system.

My plan is to list some of the predictions of the classical Drell-Yan model and to compare them with data. This discussion leads naturally to questions of scaling violations, "corrections" to the classical model, and to p_T spectra, which I take up in subsequent sections.

III. PREDICTIONS OF THE CLASSICAL MODEL

1. Scaling. An immediate consequence of the form of Eq. (1), regardless of the explicit values of $q(x)$ and $\bar{q}(x)$, is the assertion of scaling, whereby an appropriately defined quantity depends only on the ratio $M/\sqrt{s}$, at fixed y or x_F. Specifically, we should find that

$$M^4 \frac{d\sigma}{dM^2 dy} = f_S\left(\frac{M}{\sqrt{s}}, y\right) . \tag{3}$$

This equation may be rewritten in a variety of ways, including, for example,

$$\frac{M^2 d\sigma}{d\sqrt{\tau} dy} = g\left(\frac{M}{\sqrt{s}}, y\right) . \tag{4}$$

Here $\tau = M^2/s$.

To test Eq. (3) [or Eq. (4)], we need precise data at several different energies $\sqrt{s}$, for values of M which exclude the resonances of the J/ψ and Υ families; i.e., the acceptable regions of dilepton mass are $4.5 \lesssim M \lesssim 9$ GeV, or $M \gtrsim 11$ GeV. For practical reasons, only the mass range $4.5 \lesssim M \lesssim 9$ GeV has been explored thus far at several different energies. Experimental acceptance also limits the values of y at which data are available at different energies.

In the reaction $pN \to \mu\bar{\mu}X$ at $y = 0.2$, the Columbia-Fermilab-Stony Brook collaboration[1] has demonstrated that scaling holds to within 20% for $M/\sqrt{s}$ values between 0.2 and 0.4, for $p_{lab} = 200$, 300, and 400 GeV/c. Their target N is Platinum, 60% neutrons and 40% protons. This is the most precise test of scaling thus

far. A previous investigation was made by a Chicago-Princeton group.[4] Obviously tests are desirable over a wider range of s, and for more values of y. In Fig.2, I compare some recent ISR data[5] with a scaling curve derived from the 400 GeV/c pN data of the Columbia-FNAL-SUNY group.[6] The comparison does not test scaling inasmuch as the ISR data are by and large limited to $M/\sqrt{s} < 0.2$, whereas the FNAL data are in the different range $0.2 < M/\sqrt{s} < 0.5$. Within the rather large errors of the present ISR data, the comparison in Fig.2 suggests that the function $f(M/\sqrt{s})$ derived from the FNAL data can be extrapolated into a lower region of $M/\sqrt{s}$ without gross error.

Scaling violations, owing to the fact that the functions $q(x)$ and $\bar{q}(x)$ are expected to be functions also of Q^2, suggest that Eq.(3) is to be replaced by the form

$$M^4 \frac{d\sigma}{dM^2 dy} = f_{NS}\left(\frac{M}{\sqrt{s}}, M, y\right). \tag{5}$$

The explicit M dependence in f_{NS} represents the scaling violation. How large should the deviations be from the perfect scaling predicted by the classical Drell-Yan model? Theorists are now trying to answer this question[7-9], and I will return to it below. To answer the question one must first devise a set of Q^2 dependent structure functions, which are consistent with the high energy deep-inelastic $\mu p \to \mu' X$ and $\nu p \to \mu X$ data, and which fit the (latest) data from $pN \to \mu\bar{\mu}X$ at one energy, say, 400 GeV/c. Then expectations can be calculated for, say, 200 GeV/c and ISR energies. Because the $Q^2(=M^2)$ values are rela-

tively large in dilepton production ($Q^2 \gtrsim 25$ GeV^2), whereas scaling violations are most pronounced for smaller $|Q^2|$ in deep inelastic processes, the interval in s over which data are compared may have to be very substantial before scaling violations are measureable in dilepton production by hadrons.

2. Quantum Number Effects. There are many tests of this nature, some more model dependent than others. I will mention only one. Consider the ratio of cross-sections $\sigma(\pi^+T_0)/\sigma(\pi^-T_0)$ for producing high mass lepton pairs when $\pi^\pm$ beams impinge on an isoscalar target T_0. The sea component of the quark and antiquark distribution functions, $q(x)$ and $\bar{q}(x)$, dies off much more rapidly as x increases than does the valence part. Thus, at large enough lepton pair masses (recall, $M^2 = sx_1x_2$), the cross section is dominated by the annihilation of a valence anti-quark in the pion beam with a valence quark in the target. The π^+ is a $(\bar{d}u)$ system and the π^- is a $(\bar{u}d)$. Therefore, we expect $\sigma(\pi^+)/\sigma(\pi^-) = (e_d/e_u)^2 = 1/4$ for large dilepton masses. The recent Chicago-Princeton data support this expectation nicely.[2]

3. Linear Dependence on A. In the model, the quarks are assumed to act incoherently in a nucleon. Thus, they should also be incoherent in a nucleus. It is evident, therefore, that the cross-section for massive lepton pair production should be proportional to A, the total number of nucleons in a nucleus. More than a prediction of the classical Drell-Yan model, this condition is a minimum requisite for applicability of the model. It seems to hold[19] for $M \gtrsim 4.0$ GeV.

4. Transverse Momentum Distributions. As remarked above, the quarks and antiquarks are assumed to carry "little" transverse momentum, and therefore the dilepton pairs should emerge with "small" p_T. Experimentally,[5] on the other hand, it is observed that $\langle p_T \rangle \simeq$ 1.2 GeV, and $\langle p_T^2 \rangle \simeq 1.9$ GeV^2 for $5 < M < 10$ GeV in pN collisions at $p_{lab} = 400$ GeV/c. The data are shown in Fig.3. Are these statements consistent? It seems obvious that quarks and antiquarks in the initial hadrons carry some non-zero $\langle k_T \rangle$ associated simply with the fact that they (several together) are confined in a region of transverse dimensions of order 1 fermi. The uncertainty principle suggests $\langle k_T \rangle \simeq 300$ MeV. This is perhaps a lower limit. More relevant for a determination of $\langle k_T \rangle$ is the fermi motion of quarks within a hadron, which is in turn associated with the inter-quark spacing. Thus, $\langle k_T \rangle \simeq 600$ MeV, or more, is not obviously an unreasonable figure to assign for the mean transverse momentum of a quark or antiquark in the initial hadron wave function. Specific (bag) models of quark confinement can be exploited[11] to refine this estimate, to suggest whether $\langle k_T \rangle$ should vary with x of the quark, and to provide predictions for possible differences between $\langle k_T \rangle_q$ and $\langle k_T \rangle_{\bar{q}}$. Turning to the data, now, if we assume that the entire experimental figure of $\langle p_T^2 \rangle = 1.9$ GeV^2 is to be associated with transverse momenta of the quarks and antiquarks in the wave functions of the incident hadrons, then we would conclude that $\langle k_T^2 \rangle_q \simeq 1$ GeV^2. [Here I have assumed $\langle k_T^2 \rangle_q = \langle k_T^2 \rangle_{\bar{q}}$]. Adopting a Gaussian distribution in k_T, I deduce $\langle k_T \rangle_q \simeq 900$ MeV (~800 MeV if exponential).

Although 50% larger than the "fermi motion" figure I quoted above, the value of 900 MeV is not outrageously large. Nevertheless, it is the judgment of many theorists[12,13] that a dynamical explanation should be sought for the "large" experimental $\langle p_T \rangle \approx 1.2$ GeV in terms of hard-scattering models, rather than the bag or confinement explanation I sketched above. In the hard-scattering approach a substantial part of $\langle p_T \rangle$ derives from the scattering of quark and gluon (or meson) constituents, such as sketched in Fig.4. In this view, the transverse momentum of the dilepton is balanced by a quark (Fig.4(a)) or gluon (4(b)) jet in the final state. I describe specific models of this type in Sec.V.

The hard-scattering and confinement explanations differ in their predictions for the s dependence of transverse momentum effects. The observed growth[1] of $\langle p_T \rangle$, at fixed $M/\sqrt{s}$, when p_{lab} is increased from 200 to 400 GeV/c is suggestive that the hard-scattering approach is important even at relatively small values of p_T. No doubt both confinement and hard-scattering components are present. In any case, the classical Drell-Yan model needs modification. I return to this issue below in Secs. IV and V.

In Fig.5, I compare the experimental distribution[6] in p_T with calculations of $Ed\sigma/d^3p$ in which I replace $q(x)$ in Eq.(1) by the factorized form[14]

$$q(x,\vec{k}_T) = x_R^{-1}\, x\, q(x) f(|\vec{k}_T|), \tag{6}$$

with $x_R^2 = \left[x^2 + 4k_T^2/s\right]$. An identical substitution is made for $\bar{q}(x)$. The forms I use for $q(x)$ and $\bar{q}(x)$ are described later,

in Eqs.(9) and (10). For $f(|\vec{k}_T|)$ I tried both Gaussian and exponential forms, with $\langle k_T^2 \rangle_q \equiv \langle k_T^2 \rangle_{\bar{q}} = 0.5 \times (1.9)$ GeV^2. The description of the 400 GeV/c data is adequate with these naive models[14] of the confinement type, but energy dependent effects are not reproduced unless $\langle k_T \rangle_q$ is chosen to be a function of s. In Fig.3, I show how $\langle p_T \rangle$ and $\langle p_T^2 \rangle$ are expected to vary with M at 400 GeV/c in these naive models. Note the kinematic rise at small M before $\langle p_T \rangle$ becomes roughly independent of M for $M \gtrsim 4$ GeV, as in the data.

5. Angular Distributions in the Classical Drell-Yan Model.[14,15,16]

In the quark-antiquark rest frame (which is also the dilepton rest frame), the angular distribution of a final lepton is predicted to have the form

$$\frac{d\sigma}{d\Omega^*} = \left[1 + \alpha \cos^2\theta^*\right], \tag{7}$$

with

$$\alpha = \left\langle \frac{M^2 - 4m_q^2}{M^2 + 4m_q^2} \right\rangle \quad . \tag{8}$$

The average is taken over the different quark masses m_q. In the (usual) limit $M >> m_q$, $\alpha \equiv 1$. The longitudinal direction ($\theta^* = 0$) is defined by the quark-antiquark collinear axis. If the quark and antiquark carry no transverse momentum, as in the classical Drell-Yan model, then Eq.(7) is true also in the "t-channel" dilepton rest frame, in which the $\theta^* = 0$ axis is specified by the (longitudinal) direction of the initial hadrons.

Owing to the fact that $\langle p_T \rangle \neq 0$, Eq.(7) with $a = 1$, should no longer hold in the t-channel frame (and even less so in the s-channel helicity frame). In general, both θ^* and ϕ^* dependences are expected. If the effective θ^* dependence is parametrized as $\left[1 + \alpha_t \cos^2 \theta_t^*\right]$, the value of α_t in the t-channel frame is expected to change with p_T, M, x_F and s of the reaction. In Ref.14, specific forms are chosen for the distributions $f(|\vec{k}_T|)$ in Eq.(6), and explicit results are presented for the variation of α_t with x_F and M. For $M > 5$ GeV, it is found that $\langle \alpha_t \rangle \gtrsim 0.8$ for all x_F; here the average is taken over p_T. The modification of $\langle \alpha_t \rangle$ due to k_T smearing is not great for large enough dilepton masses. In Fig.6 I show the expected variation of α_t with p_T, for $M = 5.5$ GeV and $x_F = 0$. These results are of both theoretical and practical interest. When sufficient data are available, they will permit another non-trivial check of the Drell-Yan mechanism. At the moment the experimental acceptance is restricted to a small region in θ_t^* about $\theta_t^* = 0$. The theoretical results may therefore be useful now in estimating corrections to the data for the limited acceptance. In Ref.6, the assumption is made that $\alpha_t = 1$ for all M and p_T. The curves in Ref.14 suggest that this assumption overestimates the cross-section $d\sigma/dMdy$ at $y = 0$ and $M = 5$ GeV by about a factor of ~1.07 relative to that at $M > 10$ GeV. Likewise, Fig.6 suggests that the assumption leads to an overestimate of the experimental cross-section at $M = 5.5$ GeV and $p_T \simeq 4$ GeV, relative to that at small p_T, by a factor of $\simeq 1.2$.

While this latter error leads to slight overestimates of $\langle p_T \rangle$ and $\langle p_T^2 \rangle$ in the data, the effect is not substantial.

6. Absolute Normalization. While predictions for the absolute dilepton yields are perhaps the most interesting for experimental comparisons, and for estimates of $W^{\pm}$ rates, they are very sensitive to model dependent assumptions about, for example, the function $\bar{q}(x)$ in Eq. (1). To be specific, suppose we consider the observable $d\sigma/dMdy$ at $y = 0$ for $pN \to \mu\bar{\mu}X$ at 400 GeV/c. At $y = 0$, $x_1 = x_2 \equiv x = M/\sqrt{s}$, and $\sigma \propto \langle q(x)\bar{q}(x)\rangle$. (For the moment I continue to ignore possible η^2 dependence). Above the J/ψ region, where $M > 5$ GeV, the Columbia-FNAL-SUNY group[6] provide data in the range $0.2 \lesssim \frac{M}{\sqrt{s}} \lesssim 0.5$. Unfortunately, $\bar{q}(x > 0.2)$ is essentially unknown. Gargamelle neutrino data[17] at low energies provide $\bar{q}(x)$ for $x \lesssim 0.2$, and theoretical extrapolations are necessary for estimates of $\bar{q}(x > 0.2)$. Various such extrapolations have been made.[18,19] I think it is fair to say that none was successful in predicting the dimuon rate observed by the Columbia-FNAL-SUNY group[6]. One example, due to Field and Feynman[18], is compared with the data in Fig. 7. The Field-Feynman expectation falls below the data by about a factor of 3 at $M \sim 5$ GeV, but appears to meet the data for $M \gtrsim 10$ GeV. A second ingredient in the prediction of the absolute cross-section is the color factor of 3 in Eq. (1). If it were removed, the Field-Feynman curve would agree with the data at $M \approx 5$ GeV and exceed experiment at larger values of M. However, few theorists would seriously suggest dropping the color factor. Owing to present uncertainty in our knowledge of $\bar{q}(x)$ in the relevant x range, it is impossible to "test"

whether the color factor is correct in Eq.(1). This situation may change in the next year or so when good determinations are available of $\bar{q}(x)$ from neutrino counter experiments. For the time being it is more sensible to retain the color factor and to await improvements in $\bar{q}(x)$. It may be remarked that the classical Drell-Yan model has done astonishingly well in coming within a mere factor of 3 of the experimental rate. Indeed, the data themselves[6] are assigned a systematic uncertainty of 15% and a separate overall normalization uncertainty of 25%.

Given the sensitivity of the data to $\bar{q}(x)$, the problem can be inverted, and the data on $pN \to \mu\bar{\mu}X$ used to determine an average $\bar{q}(x)$. (The average here is over quark flavors and Q^2). This procedure requires an independent determination of $q(x)$, from some other source, since $\sigma_{\mu\bar{\mu}} \propto \langle q(x)\bar{q}(x)\rangle$. One method was chosen by the authors of Ref.6, who find $\bar{q}(x) \approx 0.6\ (1-x)^{10}$. I use a different procedure. I adopt Field and Feynman's parametrization of the valence part of $q(x)$, which they determine from deep-inelastic electron data. For each quark flavor, I write

$$q(x) = q_v^{FF}(x) + S(x) \tag{9}$$

$$x\bar{q}(x) = xS(x) \equiv c_1(1-x)^{c_2} \tag{10}$$

I determine that a good fit to the dimuon data is obtained if the average sea is parametrized as

$$xS(x) = 0.42(1-x)^9 \tag{11}$$

This function is determined by data in the range $0.2 < x < 0.5$.

My fit is shown in Fig.7. I attribute no virtues to this "hybrid" model, but it does provide a set of quark and antiquark distribution functions which I need for calculations reported in Sec.V. The complete details of my parametrization are provided in Table 1. The parametrization satisfies various desirable sum rules.

Several reasons may be advanced for the differences between my sea distribution and that of Field and Feynman who use $x\bar{u}(x) = 0.17(1-x)^{10}$ and $x\bar{d}(x) = 0.17(1-x)^{7}$. First, as remarked above, the Field-Feynman choices are pinned to data at $x < 0.2$, whereas my expression fits (different) data for $x > 0.2$. It is easy to concoct a form for $xS(x)$ which has the "Gargamelle value" 0.17 at $x = 0$, chosen by Field and Feynman, but which yields my expression in the range $x > 0.2$. This procedure is tantamount to suggesting that the Gargamelle and Drell-Yan sea distributions are not really different, but that they can be made to merge into one another if sufficient flexibility is adopted in parametrizing the function $xS(x)$. On the other hand, the difference can be viewed instead as a real physics difference associated with Q^2 dependence. This is the more popular theoretical interpretation. The Gargamelle data are confined to values of $|Q^2| < 2$ GeV^2, whereas in the dimuon data $25 < Q^2 < 150$ GeV^2. If $\bar{q}(x)$ is replaced by the scaling violating form $\bar{q}(x,Q^2)$, then there is no reason to suppose that the Gargamelle $\bar{q}(x,Q^2)$ should apply for values of Q^2 more than an order of magnitude larger. It is more relevant then to compare the average $\bar{q}(x)$ extracted from the dimuon data with antiquark distributions deduced from very high energy neutrino

experiments. Recent BEBC data[20] are in fact consistent with my Eq.(11). I will return to scaling violations in Sec. IV.

7. Distributions in x_F and y. The expected rapidity y and Feynman x_F dependences of $d\sigma/dMdy$ and $d\sigma/dMdx_F$ are straightforward predictions of the classical Drell-Yan model once specific forms are chosen for $q(x)$ and $\bar{q}(x)$. I've discussed uncertainties associated with $\bar{q}(x)$ above; they are reflected in expectations for the y and x_F variations of the dilepton yield.

IV. CRITIQUE OF THE CLASSICAL MODEL

In Sec. III, I surveyed some of the successes of the classical Drell-Yan model. Rather than continue in that vein, I think it is appropriate to discuss the justification for the model and to ask what modifications or reinterpretations are necessary in the light of other recent experimental and theoretical developments. I mentioned that the "large" values observed for $\langle p_T \rangle$ in $pN \to \mu\bar{\mu}X$, and the observed energy dependence of $\langle p_T \rangle$, require modifications of the classical model. I also referred to the scaling violations which appear to have been observed in high energy deep inelastic muon scattering[21] $\mu p \to \mu' X$, and by the BEBC collaboration[20] in $\nu p \to \mu X$. These data suggest that the structure functions $q(x)$ and $\bar{q}(x)$ in Eq. (1) may have to be replaced by functions with explicit Q^2 dependence, which may or may not be identical to these determined in deep inelastic reactions at $Q^2 < 0$. Moreover, we may also ask what is special about the $q\bar{q}$ annihilation diagram in Fig. 1. Why not calculate and include other contributions, for example, from the graphs shown in Fig. 4?

To first order in the strong coupling constant α_s, the constituent scattering portions of Fig. 4 are provided by the (two body final state) "quark exchange" Compton and annihilation amplitudes shown in Fig. 8. Higher order graphs may also be drawn. Those in Fig. 9, with three particle final states (q,q,γ), are typical of graphs of order $(\alpha_s)^2$. [In Figs. 8 and 9, the dilepton (not drawn) emerges, as always, from the

decay of the virtual photon]. Although $\alpha_s \propto 1/\log Q^2$, the cross section corresponding to the graphs in Fig.8 is proportional to $\alpha_s \log Q^2$, and the graphs in Fig.9 provide contributions proportional to $(\alpha_s \log Q^2)^2$. Therefore, the higher order terms are not necessarily small with respect to the simple annihilation graph in Fig.1. They may also provide different x_F and M dependences. Noting that the graph in Fig.9(a) involves the scattering of valence quark constituents, we may wonder why it is not the dominant contribution, especially in pN collisions where the annihilation diagram in Fig.1 feeds on the relatively small antiquark sea. The process sketched in Fig.9(a), where the final photon may be joined to any of the four quark lines, was in fact proposed to explain high mass dilepton production by Berman, Levy, and Neff[22] at about the same time as the original Drell and Yan proposal.

If the various diagrams sketched and suggested in Figs.8 and 9 must be computed separately then, at the very least, the "model" becomes cumbersome and may lose considerable predictive power. The amplitudes of different orders of α_s should be added coherently, before cross-sections are computed. Otherwise, errors of "double-counting" are committed. The latter difficulty can be avoided only at the price of a different or additional ambiguity; one may try to compare different constituent scattering terms with data in different regions of phase space where the amplitudes have negligible overlap (e.g. try to separate the two jet, three jet, four jet, etc. contributions).[12]

Fortunately, there is growing support among theorists for the conjecture[23] that the three problems mentioned above (scaling violations, large $\langle p_T \rangle$, and additional diagrams) are all part of the same story, and that they may be resolved together. Stated in oversimplified fashion, the idea is that the full series of constituent scattering diagrams, to all orders in α_s, generates Q^2 dependence of the structure functions, as in deep inelastic scattering. Thus, the cross-section for lepton pair production in hadron collisions, $d\sigma/dMdy$, may be computed from the simple annihilation graph in Fig.1(a), provided that Q^2 dependent structure functions are used. Moreover, these Q^2 dependent structure functions are identically those determined in deep inelastic electron, muon, and neutrino scattering at the same $|Q^2|$. In this fashion, for $d\sigma/dMdy$, effects of the higher order graphs are automatically included. When the experimentally extracted Q^2 dependent quark and antiquark distribution functions are used in Eq.(1), constituent subprocesses such as those sketched in Figs.8 and 9 should not be calculated independently, as they are already included.

The original papers[24] should be consulted for a full discussion of scaling violations in deep inelastic processes and their interpretation in terms of asymptotically free QCD. I limit myself to a few qualitative comments. In deep inelastic scattering, the quark distribution functions represent not only the naive quark model contribution sketched in Fig.10(a), but include also other effects to all orders in the strong coupling constant α_s. The "extra" contributions to first order in α_s

are illustrated in Figs.10(b) and 10(c). In Fig.10(b), the quark "first" radiates a gluon before scattering from the $Q^2 < 0$ exchanged photon and in 10(c), a gluon constituent dissociates into a quark-antiquark pair, one of which then scatters from the photon. The first order graphs in Figs.10(b) and 10(c), and those in higher order in α_s, are understood to generate Q^2 dependence of the structure functions $q(x)$. If the quark, antiquark, and gluon distributions are supplied (as functions of x) at one initial starting value $Q^2 = Q_0^2$, then the renormalization group equations of the theory provide the x distributions at higher values of $|Q^2|$. These x distributions generally change with Q^2. For example, as $|Q^2|$ grows, the valence quark distributions are predicted to become more sharply peaked toward $x = 0$. The sea distributions are expected to increase in magnitude at $x = 0$, but to fall off more sharply with increasing x. This behavior of the sea is illustrated in Fig.11. The pattern and size of the predicted Q^2 dependence (scaling violations) agree qualitatively with experiment.[24]

The obvious similarity between the graphs in Figs. 4 and 8, and those in Figs.10(b) and (c), encourages the conjecture mentioned above that the QCD Q^2 dependent corrections to the structure functions are the same in both deep inelastic processes and in lepton pair production reactions. However, the mathematical techniques available in the $Q^2 < 0$ deep-inelastic regime are inapplicable in the $Q^2 > 0$ domain of lepton pair production.

A check of the conjecture must be made in perturbation theory, order by order. It is not obvious that the necessary factorization can be demonstrated whereby a Drell-Yan type annihilation formula will result in each order of α_s. After a computation is made of the QCD diagrams, such as shown in Figs.8 and 9, it is necessary that the answer have the appearance of a product of terms, each associated with one of the initial hadrons, and that no leading terms appear involving the sum $(p_1+p_2)^2$ of the initial hadron momenta.

The quark-gluon diagrams of Fig.8(a) and (b) provide a leading contribution to the lepton pair cross-section having the form[23]

$$\sigma_0\left(1-2x_1(1-x_1)\right)\alpha_s \log(Q^2/p_1^2)$$

where p_1^2 is the four momentum of the initial gluon, and σ_0 is the classical Drell-Yan cross-section. The term multiplying σ_0 above is exactly the first term of the series for $P_{\bar{q}/G}(x,Q^2)$ representing the antiquark content of the gluon, as measured in the deep inelastic process in Fig.10(c). Thus, to this order in α_s, the contributions of Fig.8(a) and (b) are already included in the annihilation process of Fig.1 if in Eq.(1) we make the replacement

$$\bar{q}(x) \to \bar{q}(x) + P_{\bar{q}/G}(x,Q^2), \tag{12}$$

or, more generally,

$$\bar{q}(x) \to \bar{q}(x,Q^2) \ . \tag{13}$$

The gluon-gluon graphs shown in Figs.9(b) and 9(c) provide a leading contribution to the lepton pair cross-section having the form

$$\sigma_0\left(1 - 2x_1(1-x_1)\right)\left(1 - 2x_2(1-x_2)\right)\alpha_s^2 \log\left(Q^2/p_1^2\right) \log\left(Q^2/p_2^2\right) . \tag{14}$$

This expression manifests the necessary factorization, and is exactly the order α_s^2 term in the product

$$P_{q/G}(x_1,Q^2)P_{\bar{q}/G}(x_2,Q^2) . \tag{15}$$

In summary, the conjecture is that the Drell-Yan quark-antiquark annihilation formula is fully justified in a QCD framework, and that it includes in principle the sum of QCD graphs to all orders in α_s, provided that Q^2 dependent structure functions are used in Eq.(1). Moreover, these structure functions are identically those extracted from deep-inelastic processes (with a trivial change of the sign of Q^2). Thus far, this important conjecture has been verified in perturbation theory only to order $(\alpha_s)^2$ and, then, only for the leading logarithmically divergent contribution in each order. [Conceivably the "non-leading" contributions in each order in α_s are different in deep-inelastic and in massive lepton pair production processes. However, estimates given below in Sec. V suggest that the non-leading terms in order α_s are negligible].

It is of substantial interest to check the above conjecture experimentally. This requires data from deep inelastic processes of sufficient precision to allow extraction of the structure

functions $q(x,Q^2)$ and $\bar{q}(x,Q^2)$ at the same $|Q^2| > 25$ GeV^2 and $x = M/\sqrt{s}$ values at which data are taken in lepton pair experiments. For the time being, the conjecture instructs us to regard structure functions extracted from lepton pair data, as in Sec. III.6, as effectively as Q^2 dependent. Thus, the average sea distribution $0.42(1-x)^9$ in Sec. III.6 is one appropriate in the range $5 \lesssim Q \lesssim 12$ GeV. That this sea distribution has a greater intensity at $x = 0$ than the lower Q^2 Gargamelle sea is consistent with the QCD expectations illustrated in Fig.11.

Returning to the three problems mentioned at the start of this section, we see that Q^2 dependent structure functions should indeed be used in the Drell-Yan annihilation formula. They should be the same ones measured in deep-inelastic reactions. Second, the various constituent scattering graphs drawn in Figs.8 and 9 are not neglected. They generate the Q^2 dependence of structure functions, and they are automatically included in the annihilation term of Fig.1 when Q^2 dependent structure functions are used. Finally, a unique prediction of QCD graphs, such as those drawn in Figs.8 and 9, is that they generate relatively large transverse momenta. This leads to an answer to our third problem, as discussed in the next section, and relates the size of scaling violations to $\langle p_T \rangle$.

V. TRANSVERSE MOMENTUM DISTRIBUTIONS

In Section III.4 I discussed briefly the available data on transverse momentum distributions and introduced possible interpretations. Two contributions to the transverse momentum (p_T) of the lepton pairs may be identified. I label one of these components the "confinement" piece. Because the quark, antiquark, and gluon constituents are confined in an initial hadron of finite size, they have some distribution in their transverse momenta k_T, with $\langle k_T \rangle \simeq 600$ MeV, as discussed in Sec. III.4. When these distributions in k_T for the quark and antiquark are introduced into Eq.(1), and convoluted as in Ref.14, the lepton pairs are produced with non-zero $\langle p_T \rangle$, as shown in Figs.3 and 5. The second component of the p_T distribution is the "hard scattering" part. If the constituents scatter "before" the virtual photon is emitted, as in Figs.4, 8, and 9, the photon emerges with relatively large p_T. In the hard-scattering approach, the bulk of the transverse momentum of the photon is balanced by a jet of hadrons from the recoiling quarks or gluons, as sketched in Fig.12. (If asymptotically free QCD can also be shown to lead to confinement, then the two components I have distinguished are really not distinguishable. Since proof of confinement does not exist, I will assume that the confinement and hard scattering contributions are physically distinct. They may also be distinguished experimentally).

1. Confinement. In Sec. III, Fermi motion arguments were

used to estimate that confinement provides $\langle k_T \rangle_q \approx 600$ MeV. Similar reasoning would suggest that quarks and antiquarks in the sea have greater values of $\langle k_T \rangle$ than the valence component. This idea could be tested most directly by a comparison of $\langle p_T \rangle$ in $\bar{p}N$ and pN reactions. Because the $\bar{p}N$ process is dominated by valence-valence annihilation, we should find $\langle p_T \rangle_{\bar{p}p} < \langle p_T \rangle_{pp}$. Unfortunately, it is unlikely that data will be available soon from $\bar{p}N \to \mu\bar{\mu}X$ with values of $M > 5$ GeV. The reaction $\pi N \to \mu\bar{\mu}X$ is also dominated by valence-valence annihilation at large enough values of M. However, comparisons with pN reactions are difficult because confinement estimates are likely to be different for pion and proton systems. The data[2] indicate that $\langle p_T \rangle_{\pi N} > \langle p_T \rangle_{pp}$ at the same lepton pair masses and beam energies (at 225 GeV/c, $\langle p_T \rangle_{\pi N} \approx 1.2$ GeV; at 200 GeV/c, $\langle p_T \rangle_{pp} \approx 1.0$ GeV, both for $M > 4$ GeV). Another question concerns the possible x dependence of $\langle k_T \rangle$. This uncertainty translates into uncertainty about the expected M and x_F dependences of $\langle p_T \rangle$. The simple factorized form chosen in Eq. (6) is surely not correct, but its "prediction" that $\langle p_T \rangle$ is independent of both M and x_F does agree with, for example, the $\pi p \to \mu\bar{\mu}X$ data[2] at 225 GeV, where $\langle p_T \rangle$ is independent of x_F over the large range $0 < x_F < 0.6$. It would be valuable to have specific predictions from confinement (bag) model calculations to compare with the data.

One point on which the confinement and hard scattering approaches differ is in their expectations for the s dependence of the p_T distribution. If both x_F and $M/\sqrt{s}$ are fixed, then the quark and antiquark longitudinal fractions x_1 and x_2 are

fixed in Eq.(1). Under these conditions, confinement models should predict that $\langle p_T \rangle$ is independent of s. This is not true in the hard scattering approach, as described below, and it appears not to be true in the data either[1]; c.f. Fig.13.

2. Hard Scattering Component.[12,13] Because QCD is not a soft field theory, there is no cutoff in the model, and $\langle p_T \rangle$ increases in unbounded fashion with whatever momentum variable sets the dynamical scale. It is expected, therefore, that $\langle p_T^2 \rangle$ should have the form[13]

$$\langle p_T^2 \rangle = a + b\, M^2/\log (M^2/\Lambda^2) \ . \tag{16}$$

Here a and b are functions of the dimensionless ratio $M/\sqrt{s}$. The function a is the confinement contribution, and the term $b\, M^2/\log (M^2/\Lambda^2)$ represents the QCD expectation. The scale parameter Λ of the theory is in the range 0.5 to 1 GeV. The full M dependence of Eq.(16) requires knowledge of $b(M/\sqrt{s})$ which may be calculated explicity from QCD diagrams, as shown below. Since $\langle p_T^2 \rangle$ is observed[1,2] to be nearly independent of M in the range $5 < M < 12$ GeV, b must be roughly of the form (s/M^2) in this range of M.

Based on his QCD calculations, Politzer[13] proposed that quarks and antiquarks be assigned the mean transverse momentum

$$\langle k_T^2 \rangle_q \approx 0.09 + \frac{M^2(1-x)}{16 \log (M^2/\Lambda^2)} \ , \tag{17}$$

with $\Lambda = 0.5$ GeV. At $x_F = 0$, $x = M/\sqrt{s}$, and, therefore, Politzer's

approximation for b in Eq.(16) is

$$b = \frac{1}{8}(1 - M/\sqrt{s}) \ . \qquad (18)$$

At 400 GeV/c and $x_F = 0$, this prediction provides a curve for $\langle p_T^2 \rangle$ versus M which rises almost linearly from 0.7 GeV^2 at M = 5 GeV to 1.9 GeV^2 at M = 13 GeV, in clear disagreement with the data shown in Fig.3(b). Politzer's approximation was based on an analytic approximation to the QCD graphs, valid only in the limit $x \to 1$. Since the data lie in the range $0.2 < x < 0.5$, the disagreement is not surprising. As described below, a complete numerical study of the same graphs leads to more satisfactory agreement with experiment.

Beginning with Eq.(16) and dropping the slowly varying $\log M^2$ factor, we may deduce that

$$\langle p_T^2 \rangle = a + \tilde{b}\, s \ , \qquad (19)$$

where $\tilde{b} \equiv M^2 b/s$ is a new function of $M/\sqrt{s}$. We conclude that at fixed $M/\sqrt{s}$ the QCD portion of $\langle p_T^2 \rangle$ is predicted to grow linearly with s. This may be contrasted with the expectation of a constant $\langle p_T^2 \rangle$ from confinement.

Data available on the energy dependence of $\langle p_T \rangle$ in lepton pair production at $y \approx 0$ are shown in Fig.13. The Fermilab data[1] from 200 to 400 GeV/c show the rise expected in the hard scattering approach. The ISR data[5] are taken at a different value of $M/\sqrt{s}$, and a direct comparison with the Fermilab results is therefore not possible. However, a rather large variation in the $M/\sqrt{s}$ dependence of $\tilde{b}$ in Eq.(19) would be required to accommodate both the FNAL and ISR results. It will be interesting to see whether the values of $\langle p_T \rangle$ observed at the ISR increase when greater statistics are accumulated.

3. Explicit Calculations. I turn now to an explicit calculation of the contributions of the hard-scattering graphs shown in Figs.4 and 8. Graphs similar to those in Fig.8 give rise to three-jet events in $e^+e^- \to$ hadrons and in deep inelastic processes such as $\mu p \to \mu' X$. Here I am interested in the contribution which the graphs make to the p_T distribution of dileptons in $h_1 h_2 \to \ell^+ \ell^- X$.

After a sum over the spins of the final quark and of the two leptons, an integral over the phase space of the lepton pair, and an average over the initial quark and gluon spins, the absolute square of the sum of the Compton scattering amplitudes in Figs.8(a) and (b) is found to be[25]

$$|A_C^i|^2 \equiv \frac{1}{4\pi} \int \sum_{\substack{\text{spins,} \\ \text{color}}} |M_{\text{COMPTON}}|^2 \, d\Omega_{\ell^+\ell^-}$$

$$= \frac{4}{9} c_{qi}^2 (4\pi)^3 \alpha^2 \alpha_s \left[\frac{-2M^4 + 2M^2(\hat{u}+\hat{s}) - (\hat{u}^2+\hat{s}^2)}{\hat{s}\,\hat{u}\,M^2} \right] \qquad (20)$$

Included in Eq.(20) is the appropriate factor (1/6) for the sum and average over color indices. The fractional charge $|c_{qi}|$ of the quark has the values $(\frac{2}{3}, \frac{1}{3}, \frac{1}{3})$ for the $i = (u,d,s)$ quarks. The variables $\hat{s}$ and $\hat{u}$ are indicated in Fig.8(a): $\hat{s} = (p_q + p_G)^2$, and $\hat{u} = (p_\gamma - p_q)^2$. I assume that the quarks and the gluon are massless. The constant $\alpha = 1/137$, and in this report I fix $\alpha_s = 0.3$, independent of Q^2. My results are not changed in any significant way if I instead choose $\alpha_s \propto 1/\log(Q^2/\Lambda^2)$.

After a sum over final spins, an average over initial spins, and an integration over the phase space of the lepton pair, the absolute square of the sum of the annihilation amplitudes in Figs.8(c) and 8(d) yields

$$|A_A^i|^2 = \frac{1}{4\pi}\int \sum_{\substack{\text{spins,}\\ \text{color}}} |M_{\text{Annih.}}|^2 \, d\Omega_{\ell^+\ell^-}$$

$$= \frac{32}{27} c_{qi}^2 (4\pi)^3 \alpha^2 \alpha_s \left[\frac{-2M^4 + 2M^2(\hat{t}+\hat{u}) - (\hat{u}^2+\hat{t}^2)}{-\hat{t}\,\hat{u}\,M^2}\right] . \qquad (21)$$

Again, the appropriate factor (4/9) for the sum over color indices is included in Eq.(21). The variables $\hat{t}$ and $\hat{s}$ are indicated in Fig.8(c); $\hat{s}+\hat{t}+\hat{u} = M^2$. Note that the definitions of $\hat{s}$, $\hat{t}$, and $\hat{u}$ differ in Figs.8(a) and 8(c).

The cross-section $d\sigma/dM^2 d\hat{u}$ for the process $q_i G \to (\ell^+\ell^-)q_i$ is obtained directly from Eq.(20) as

$$\frac{d^2\sigma_i^C}{dM^2 d\hat{u}} = \left(\frac{1}{2\pi}\right)^4 \frac{\pi}{16\hat{s}^2} |A_C^i|^2 . \qquad (22)$$

Likewise, the cross-section for the process $q_i\bar{q}_i \to (\ell^+\ell^-)G$ is obtained directly from Eq.(21) as

$$\frac{d^2\sigma_i^A}{dM^2 d\hat{t}} = \left(\frac{1}{2\pi}\right)^4 \frac{\pi}{16\hat{s}^2} |A_A^i|^2 \qquad (23)$$

Quark, lepton, and gluon masses have all been neglected in Eqs.(22) and (23).

To find the contribution of the Compton graphs to $h_1 h_2 \to$

$\ell^+\ell^- X$, the expression in Eq. (22) must be multiplied by the probabilities that quark and gluon constituents in the initial hadrons carry longitudinal momentum fractions x_1 and x_2, respectively, and then an integral performed over inessential variables. I find

$$d\sigma(h_1 h_2 \to \ell^+\ell^- X) = \int d^2k_{T1}\, dx_1\, d^2k_{T2}\, dx_2\, P_{qi/h1}(x_1, \vec{k}_{T1})$$

$$P_{G/h2}(x_2, \vec{k}_{T2}) \left(\frac{d^2\sigma_i^C}{dM^2 d\hat{u}}\right) dM^2 d\hat{u} + (1 \leftrightarrow 2) \ . \qquad (24)$$

In discussing the hard scattering contribution in this report, I shall ignore the transverse momenta associated with confinement. I set $P_{q/n1} = q(x_1)\delta(\vec{k}_{T1})$ and $P_{G/h2} = G(x_2)\delta(\vec{k}_{T2})$. Smearing effects in the p_T spectra associated with the finite values of $\langle k_{T1} \rangle$ and $\langle k_{T2} \rangle$ are therefore ignored here. The gluon probability $G(x_2)$ is specified below.

Transforming variables in the integrand of Eq. (24), I find that

$$dx_1 dx_2 d\hat{u} = \frac{x_1 x_2 dx_F dp_T^2 dx_q}{\left[x_F^2 + \frac{M^2+p_T^2}{P^2}\right]^{\frac{1}{2}} \left[x_q^2 + \frac{p_T^2}{P^2}\right]^{\frac{1}{2}}} \ . \qquad (25)$$

Here P is the c.of.m. momentum of the overall collision ($P \approx \sqrt{s}/2$), and x_q is the fraction of longitudinal momentum carried by the final unobserved quark. The Eq. (25) may also be written as

$$dx_1 dx_2 d\hat{u} = \frac{x_1 x_2 dy dp_T^2 dx_q}{(x_q^2 + p_T^2/P^2)^{\frac{1}{2}}} \tag{26}$$

Combining Eqs. (20), (22), (24), and (26), I obtain the following contribution from the Compton graphs to $h_1 h_2 \to \ell^+ \ell^- X$

$$\frac{d\sigma^C}{dM^2 dp_T^2 dy} = \sum_{i=1}^{3} \int \frac{dx_q}{\left[x_q^2 + p_T^2/P^2\right]^{\frac{1}{2}}} x_1 \left[q_i(x_1) + \bar{q}_i(x_1)\right] x_2 G(x_2) \frac{d^2\sigma_i^C}{dM^2 d\hat{u}} + (1 \leftrightarrow 2) \tag{27}$$

In Eq. (27), M, p_T, and y are the mass, transverse momentum, and rapidity of the pair of leptons. Note that in Eq. (27) I include the contributions of both $\bar{q}G \to \gamma\bar{q}$ and $qG \to \gamma q$. The first term of the equation represents the process in which the quark or antiquark emanates from hadron 1 and the gluon from hadron 2. These roles are interchanged in the term $(1 \leftrightarrow 2)$. The variables $\hat{s} = x_1 x_2 s$ and $\hat{u}$ in the explicit expression for $d^2\sigma/dM^2 d\hat{u}$ in Eq. (27) may be reexpressed easily in terms of my chosen set M^2, p_T^2, y and x_q. This transformation differs slightly for the second term $(1 \leftrightarrow 2)$. The integral over x_q in Eq. (27) runs over both positive and negative values of x_q. With some care, this integration can be handled well numerically.

For the annihilation process, in which $h_1 h_2 \to \ell^+ \ell^- X$ via the process $q\bar{q} \to G\ell^+\ell^-$, I derive

$$\frac{d\sigma^A}{dM^2 dp_T^2 dy} = \sum_{i=1}^{3} \int \frac{dx_q}{\left[x_q^2 + p_T^2/P^2\right]^{\frac{1}{2}}} x_1 q_i(x_1) x_2 \bar{q}_i(x_2) \frac{d^2\sigma_i^A}{dM^2 d\hat{t}} + (1 \leftrightarrow 2) \tag{28}$$

The first term of Eq.(28) represents the process in which the quark emerges from hadron 1 and antiquark from hadron 2. These roles are reversed in the term $(1 \leftrightarrow 2)$.

Results in millibarn units are obtained after the factor 0.3893 is inserted on the right hand side of Eqs.(27) and (28).

4. Scaling Properties. It is instructive to examine the behavior of Eqs.(27) and (28) as functions of s and p_T. For the Compton scattering process, after introducing the c.of.m. scattering angle θ between the initial quark and final virtual photon, I reexpress

$$\hat{u} = -\frac{1}{2}(\hat{s} - M^2)(1 - \cos\theta) , \tag{29}$$

and

$$p_T = \frac{1}{2\sqrt{s}} (\hat{s} - M^2) \sin\theta . \tag{30}$$

The scaled transverse momentum x_T is defined as

$$x_T = 2p_T/\sqrt{s} . \tag{31}$$

Note that $\sin\theta$ [or $\cos\theta$] is a function of the scaling variables x_T, $M/\sqrt{s}$, and of x_1 and x_2. Rewriting Eq.(29), I obtain

$$\hat{u} = -p_T^2 \frac{2\hat{s}}{(\hat{s} - M^2)(1 + \cos\theta)} . \tag{32}$$

The Compton scattering matrix element, Eq.(20) may therefore be expressed as

$$|A_C^i|^2 = \frac{1}{p_T^2} g_C(x_T, M/\sqrt{s}, x_1 x_2) , \tag{33}$$

where the function g_C depends only on scaled quantities x_T, $M/\sqrt{s}$, x_1 and x_2. Likewise, the annihilation matrix element, Eq.(21), may be written as

$$|A_A^i|^2 = \frac{1}{p_T^2} g_A(x_T, M/\sqrt{s}, x_1 x_2) . \tag{34}$$

Analyzing the Eqs.(27) and (28) in similar fashion, I find that

$$\frac{d\sigma^C}{dM^2 dp_T^2 dy} = \frac{1}{s^2 p_T^2} f_C(x_T, M/\sqrt{s}, y) \ , \tag{35}$$

and

$$\frac{d\sigma^A}{dM^2 dp_T^2 dy} = \frac{1}{s^2 p_T^2} f_A(x_T, M/\sqrt{s}, y) \ . \tag{36}$$

The factor s^{-2} in Eqs.(35) and (36) comes from the $\hat{s}^{-2}$ factor in Eqs.(22) and (23). The functions f_C and f_A depend only on y and on the scaling variables x_T and $M/\sqrt{s}$. Both f_C and f_A are regular as $p_T \to 0$.

The Eqs.(35) and (36) show that the Compton and annihilation cross-sections diverge as p_T^{-2} as $p_T \to 0$. This (infra-red) behavior is evident in the explicit numerical results shown in Fig.14, and I will return to its ramifications below.

In the classical Drell-Yan model discussed in Secs.II and III, the scaling prediction is of the form:

$$\underline{\text{Classical Model Scaling}} \qquad s^2 \frac{d\sigma}{dM^2 dy} = f_0(M/\sqrt{s}, y) \ . \tag{37}$$

Presumably at fixed small p_T, in the region of transverse momentum where confinement effects control the p_T spectrum, Eq.(37) is replaced by

$$s^2 \frac{d\sigma}{dM^2 dy dp_T^2}\bigg|_{\text{small } p_T} = \tilde{f}_0(M/\sqrt{s}, y, p_T) \ . \tag{38}$$

By contrast, in the hard-scattering region, where the Compton

and annihilation processes are dominant, the Eqs.(35) and (36) demonstrate a very different scaling form:

$$\underline{\text{Hard-Scattering Scaling}} \qquad s^3 \frac{d\sigma}{dM^2 dp_T^2 dy}\bigg|_{\text{large } p_T} = f_1(M/\sqrt{s}, y, x_T) \ . \tag{39}$$

The s^2 factor of Eq.(38) is replaced by s^3, and the p_T dependence on the right hand side of the equation enters as a dependence on $x_T = 2p_T/\sqrt{s}$.

The Eq.(39) is a general consequence of the hard-scattering assumption, and its verification in the data for $p_T \gtrsim 1$ GeV is a critical test of whether the hard-scattering mechanism is responsible for the "large" values of $\langle p_T \rangle$ seen in massive lepton pair production. In the "confinement" or "infra-red" region of $p_T \lesssim 1$ GeV, the classical form Eq.(38) may hold. However, for $p_T > 1$ GeV the hard-scattering expectation Eq.(39) should set in. Tests of the hard-scattering prediction in massive lepton pair production should be cleaner than in high-p_T hadron production reactions because in the lepton pair process the whole jet is always captured. Absent are the complicated smearing effects associated with the quark decay into hadrons.[26]

The different energy dependences represented by Eqs.(38) and (39) are illustrated in Fig.15. I have plotted the explicit numerical results of my QCD calculations, which satisfy Eq.(39) perfectly, as a function of p_T, for fixed $M/\sqrt{s} = 0.265$. If the QCD explanation is correct, the cross-section $s^2 d\sigma/dM^2 dy dp_T^2$ in the reaction $pN \to \mu\bar{\mu}X$ at $M/\sqrt{s} = 0.265$ and $y = 0$ should increase by a healthy factor of 3 at $p_T = 2.5$ GeV when the lab

momentum is increased from 200 to 400 GeV/c. This dramatic prediction of the hard-scattering approach should be verified soon. It is not subject to some of the ambiguities discussed below associated with QCD predictions for the moments $\langle p_T^2 \rangle$ and $\langle p_T \rangle$.

5. Infra-Red Divergence and Comparisons with Data. I now address two problems which beset all attempts to compare calculations of QCD processes with experiment. In QCD perturbation theory, the quarks and gluons are treated as if they are free and can emerge from their parent hadrons (c.f. Fig.4), whereas in Nature they appear to be entirely confined. In comparisons with data, we must deal somehow with the non-perturbative effects which provide or are associated with confinement, or else seek tests of QCD which are insensitive to the non-perturbative effects. As discussed earlier, confinement effects are expected to be dominant at small values of p_T, but they will also cause some smearing of the p_T spectrum at large p_T. Second, perturbative QCD is subject to infra-red divergences analogous to those which are present in QED. The infra-red problem is manifested in Eqs. (35) and (36) by the p_T^{-2} divergence of the equations. When the momentum carried by the massless exchanged quark in Figs.8(a) or 8(c) vanishes (i.e. when the quark goes on-shell) the cross-section becomes infinite. These twin-problems of confinement and infra-red divergence in QCD are not unique to the lepton pair production process. They are also faced elsewhere, for example, in calculations of jet effects in $e^+e^- \rightarrow$ hadrons.[27]

One lesson of the solution of the infra-red problem in QED is that the divergences are mastered if we deal with cross-sections defined with suitable energy and angle cutoffs. This presumably will also be true in QCD.[28] When the virtual photon carries small p_T, events associated with the processes represented in Figs.4(a) and 4(b) cannot be distinguished experimentally from those due to Fig.1. At small p_T, the final quark in Fig.4(a), or the final gluon in Fig.4(b), is not outside the region of phase space populated by the constituents which have stayed behind and form the debris of the parent hadron h_2. The processes in Fig.1 and 4 are not incoherent at small p_T, and it would be improper to add cross-sections. Coherence effects are important, and one should deal with a sum of amplitudes — a problem of both infra-red and confinement complexity as yet beyond the reach of theorists.

The suitable "energy and angle cutoffs" in the problem of lepton pair production correspond to a selection of p_T larger than some critical value. Below that value, cross-sections computed in QCD perturbation theory are inapplicable not only because of their infra-red divergences, but also because of the more serious (and related) neglect of coherence and confinement effects. When the virtual photon transverse momentum is above the critical p_T, the processes represented in Fig.4 should dominate over the rapidly decreasing small p_T spectrum associated with Fig.1.

I add two final remarks before turning to a discussion of my numerical calculations. When an integral is done over p_T^2, the p_T^{-2} divergence of Eqs.(35) and (36) at small p_T gives

rise to a logarithmically divergent $\alpha_s \log(Q^2/p^2)$ contribution to $d\sigma/dM^2dy$. This is exactly the scaling violation contribution in first order in α_s, discussed in Sec. IV. Second, in a somewhat different hard-scattering approach to massive-lepton pair production, Blankenbecler and collaborators[12] introduce a large quark mass (~1 GeV). They use diagrams similar to those in Fig.4, with the gluon replaced by a scalar meson. Owing to the large mass in the exchanged quark propagator, the p_T^{-2} divergence of Eqs.(35) and (36) is avoided. While such a large quark mass is perhaps hard to motivate, the phenomenological result is to provide a p_T distribution without a divergence near $p_T = 0$. The quark mass of 1 GeV plays the role in the Blankenbecler model of the ~1 GeV confinement cutoff which I use.

6. Specific Parametrizations and Data. To obtain specific numerical results it is necessary to choose expressions for the quark, antiquark, and gluon densities which appear in Eqs.(27) and (28). For the quark and antiquark densities I use the structure functions of the hybrid model I presented in Sec. III.6 and in Table 1. As discussed, these functions fit data in the range $M/\sqrt{s}$ from 0.2 to 0.5 GeV. While only functions of x, and thus of a scaling form, they are to be understood as effectively Q^2 dependent, valid in an average sense in the range $25 < Q^2 < 150$ GeV^2. Because the structure functions thus include some QCD "corrections" to order α_s and higher, the Compton and annihilation cross-sections I present are not purely of first order in α_s

but also include some higher order effects. There is no way to avoid this situation since there is no way to measure structure functions which do not include QCD "corrections" to all orders in α_s.

For the gluon density, G(x) in Eq.(27), I choose the parametrization

$$xG(x) = \frac{p+1}{2}(1-x)^p \ , \tag{40}$$

where the power p is the "only free parameter" of my QCD calculations. The parametrization in Eq.(40) is normalized so that 50% of the nucleon's momentum is carried by gluons. To determine the power p, I require that the QCD model yield a variation of $\langle p_T^2 \rangle$ which is independent of lepton pair mass M in the range $5 < M < 10$ GeV, as is observed in data.[6] This requirement fixes $p \approx 5$ or 6 in Eq.(40). Higher (lower) powers of p result in a decreasing (rising) curve of $\langle p_T^2 \rangle$ vs. M. The calculation of $\langle p_T^2 \rangle$ is discussed below. For all results presented in this report I fix $p = 6$.

Results of my explicit evaluation of Eqs.(27) and (28) are compared with data in Fig.14. I show data only for the mass interval $7 \leq 8 \leq 9$ GeV, but the comparison is qualitatively similar in other regions of M. Evident in Fig.14 is the p_T^{-2} divergence of the theoretical curves at small p_T. In the region $1 < p_T < 2$ GeV, the Compton and annihilation processes have comparable magnitudes; the Compton contribution is dominant at large p_T. The solid curve is obtained when the Compton and annihilation

cross sections are added incoherently. As discussed in Sec. V.5, below a given critical p_T, which I expect to be about 1 GeV, the perturbation theory curves are inapplicable. In the region $p_T < 1$ GeV, confinement effects which are outside the scope of the theory should control the experimental distribution and also remove the infra-red divergence. In the region $p_T > 1$ GeV a comparison of theory and experiment should be meaningful. Two problems are obvious in Fig.14: the theory curves are a factor of two or more below the data in absolute normalization; the shape of the curves may be qualitatively incorrect, showing upward curvature instead of the downward trend of the data. In the calculation I assume that the initial constituents in the scattering carry no transverse momentum. It remains to be shown whether smearing effects in p_T obtained by assigning non zero $\langle k_T \rangle$ to the initial quark, antiquark, and gluon constituents improve the agreement of theory and experiment significantly.

The energy dependence of the theoretical distribution is shown in Fig.15 at fixed $\tau = M^2/s = 0.07$. This value of τ is selected in order that the associated values of M be both accessible experimentally for laboratory momenta in the Fermilab and SPS energy ranges, and in the relevant continuum region of M between the J/ψ and T families. As emphasized in Sec. V.4, the factor of three increase of $s^2 d\sigma/dx_F dM^2 dp_T^2$ at $p_T \simeq 2.5$ GeV predicted by the theory is a critical test of the hard-scattering assumption. In Fig.15 the solid curves result from addition of the Compton and annihilation cross-sections.

7. Moments. In the search for theoretical variables and distributions which are insensitive to the infra-red, confinement, and other non-perturbative problems of the small p_T region, it is interesting to consider moments $\langle p_T^n \rangle$ of the p_T distribution. Owing to the relatively large statistical errors in the data at large p_T, only the first few moments ($n = 1,2$) are meaningful.

In a perturbation approach, it is expected that the cross-section $d\sigma/dM^2dy$ has an expansion in α_s of the type

$$\sigma(M,y) \equiv \frac{d\sigma}{dM^2dy} = \sigma_0(M,y) + \alpha_s\sigma_1(M,y) + \alpha_s^2\sigma_2(M,y) + \ldots \quad . \tag{41}$$

The first term in Eq.(41) represents the basic zero'th order classical Drell-Yan process of Fig.1. We may also consider the integrals

$$\left\langle p_T^n \frac{d\sigma}{dM^2dydp_T^2} \right\rangle \equiv \int p_T^n dp_T^2 \left(\frac{d\sigma}{dM^2dydp_T^2} \right) \quad . \tag{42}$$

As in Eq.(41), these have an expansion

$$\left\langle p_T^n \frac{d\sigma}{dM^2dydp_T^2} \right\rangle = \left\langle p_T^n \frac{d\sigma_0}{dM^2dydp_T^2} \right\rangle + \alpha_s \left\langle p_T^n \frac{d\sigma_1}{dM^2dydp_T^2} \right\rangle + O(\alpha_s^2) \tag{43}$$

In the approximation in which the hadron constituents carry no intrinsic transverse momentum, the first term on the right hand side of Eq.(43) is zero. The second term on the right hand side of Eqs.(41) and (43) is provided by the Compton and annihilation processes, Eqs.(27) and (28). In spite of the p_T^{-2} divergence displayed in Eqs.(35) and (36), the second term on the right hand

side of Eq. (43) is finite for all $n \geq 1$. Looking ahead to the possibility of adding later non-perturbative and confinement effects in quadrature, one is led to concentrate on the second moment, with $n = 2$. We may investigate the finite ratio R_2 defined by

$$R_2 = \frac{\alpha_s \left\langle p_T^2 \frac{d\sigma_1}{dM^2 dy dp_T^2} \right\rangle}{\sigma(M,y)} \quad . \tag{44}$$

In this ratio, the denominator is the full cross-section given in Eq. (41); it is a measured quantity. Formally, we might consider replacing $\sigma(M,y)$ in the denominator of R_2 by the zero'th order term $\sigma_0(M,y)$ of Eq. (41). This would change the value of R_2 only to order α_s^2. Thus, R_2 provides a fine definition of the first-order perturbative QCD contribution to the moment $\langle p_T^2 \rangle$.

Is R_2 a quantity which is insensitive to infra-red and non-perturbative problems? It is clear that there is no infra-red divergence in the calculation of R_2; the p_T^{-2} behavior of the cross-section is exactly compensated by the p_T^2 insertion, and the integrand is well behaved for all p_T. However, it is not so easy to dispose of other non-perturbative problems. If the lower limit of integration in Eq. (42) extends to $p_T = 0$, as is usual in the definition of moments, then some contribution to the answer necessarily comes from the non-perturbative, confinement region of $p_T < p_{T,crit} \approx 1$ GeV where the perturbative calculation is inapplicable. One way to handle this problem would be to define incomplete moments in which the integral is done only for values

of $p_T > p_{T,crit} = 1$ GeV. To make sense this would have to be done also for the cross-section appearing in the denominator of Eq. (44). In this report I set this confinement problem aside, and I adopt R_2 in Eq. (44) as the proper definition of $\langle p_T^2 \rangle$ in first order QCD, with the lower limit of integration in Eq. (42) extended all the way to $p_T = 0$.

Recalling Eqs. (35) and (36), we may derive

$$\alpha_s \left\langle p_T^2 \frac{d\sigma_1}{dM^2 dy dp_T^2} \right\rangle = \frac{1}{s^2} \int (f_C + f_A) s \frac{dp_T^2}{s} \equiv s^{-1} \tilde{f}_1(M/\sqrt{s}, y) \quad . \tag{45}$$

Inasmuch as the denominator of Eq. (44) satisfies the classical scaling property $s^2 \sigma(M,y) = f_0(M/\sqrt{s}, y)$, I conclude that

$$\langle p_T^2 \rangle_{QCD} = R_2 = s \frac{\tilde{f}_1(M/\sqrt{s}, y)}{f_0(M/\sqrt{s}, y)} \quad . \tag{46}$$

This linear growth of $\langle p_T^2 \rangle_{QCD}$ with s at fixed $M/\sqrt{s}$ was discussed above on more general grounds. The present analysis provides specific (model-dependent) predictions for the coefficient b in the general formula $\langle p_T^2 \rangle = a + bs$.

The results I obtain for $\langle p_T^2 \rangle_{QCD}$ are shown as a function of mass in Fig. 16 for the reaction $pN \to \mu\bar{\mu}X$ at 400 GeV/c and $y = 0$. For $M = 7$ GeV the Compton and annihilation processes each provide $\langle p_T^2 \rangle_{QCD} = 0.4$ GeV^2. As shown in the figure, the sum of the two QCD processes yields a curve of $\langle p_T^2 \rangle$ which rises rapidly with M, flattens off in the range $5 < M < 11$ GeV, and then begins to drop as M is increased further. As remarked earlier, the

shape of the Compton contribution to $\langle p_T^2 \rangle_{QCD}$ vs. M is influenced by the choice of the power p in Eq.(40). If I select powers smaller (larger) than my value p = 6, the Compton contribution in Fig.16 will rise faster (fall faster) with M than the result I have shown. The shape of the annihilation contribution in Fig.16 is fixed since the structure functions q(x) and $\bar{q}(x)$ are both fixed.

To my knowledge there are no other empirical determinations of the power p of the gluon distribution. If this QCD analysis of the M dependence of $\langle p_T^2 \rangle$ is accepted as a relevant constraint, the power p = 5 or 6 is determined for the first time. This power places the slope in x of the gluon distribution somewhere between those of the valence and sea quark distributions, which seems reasonable.

The net QCD contribution illustrated by the dotted line in Fig.16 represents only about one-half the experimental value of $\langle p_T^2 \rangle$ at 400 GeV/c. To reproduce the data in the range $5 < M < 10$ GeV, it is necessary to add ~1.04 GeV^2 to the QCD contribution. This addition may be associated with the non-perturbative and "confinement" contributions which I set aside above. Thus, I write

$$\langle p_T^2 \rangle = 1.04 + \langle p_T^2 \rangle_{QCD} \quad . \tag{47}$$

The confinement portion may depend on the ratio $(M/\sqrt{s})$ but should be otherwise independent of s. In this report I take it to be a pure constant. The result of the addition of the QCD and confinement effects is shown as the solid line in Fig.16.

The test of these QCD calculations and speculations lies in the energy dependence of $\langle p_T^2 \rangle$. In Fig.17, I provide my expectations for $\langle p_T^2 \rangle_{QCD}$ in the Fermilab and SPS energy range. A rather flat behavior is obtained for the dependence of $\langle p_T^2 \rangle$ vs. M at all energies. The slope b which I calculate in the expression $\langle p_T^2 \rangle = a + bs$ is shown as a function of $M/\sqrt{s}$ in Fig.18. It has a maximum value of $b \simeq 1.15 \times 10^{-3}$ GeV^{-2} for $M/\sqrt{s} \simeq 0.3$. The results of my explicit calculation of $b(M/\sqrt{s})$ do not resemble the analytic form $(1 - M/\sqrt{s})$ guessed by Politzer.[13] His form is valid perhaps in the neighborhood of $M/\sqrt{s} = 1$.

At a value of $M/\sqrt{s} \simeq 0.1$ typical of the ISR energy range, my slope is $b \simeq 0.74 \times 10^{-3}$ GeV^{-2}. Thus, at $\sqrt{s} = 52$ GeV and $M/\sqrt{s} \simeq 0.1$, I predict $\langle p_T^2 \rangle_{ISR} = 1.04 + 2.00 \cong 3$ GeV^2, and $\langle p_T \rangle_{ISR} \simeq$ 1.4 to 1.5 GeV. These predictions are about 50% higher than the ISR data shown in Fig.13. It is important to confirm the ISR measurements with data of higher statistics.

A semi-empirical method may be adopted to obtain the first moment $\langle p_T \rangle$. The experimenters[6,1] report that their data are well fitted by the expression

$$E \frac{d\sigma}{d^3p} = A(M) \left(1 + \frac{p_T^2}{\lambda^2}\right)^{-6} \tag{48}$$

where the value of λ changes with energy but not with M. This fit implies that for all λ

$$\langle p_T \rangle = \frac{35\pi}{128} \langle p_T^2 \rangle^{\frac{1}{2}} = 0.859 \langle p_T^2 \rangle^{\frac{1}{2}} \quad . \tag{49}$$

Starting with my results for $\langle p_T^2 \rangle = 1.04 + \langle p_T^2 \rangle_{QCD}$, and using the "experimental" Eq.(49), I derive the values of p_T shown in Fig.19. The agreement with the data at 400 GeV is excellent (by construction). The new feature of Fig.19 is the prediction of $\langle p_T \rangle_{th} \approx 1.03$ GeV at 200 GeV. This is in fine agreement with the experimental value[1] of $\langle p_T \rangle_{exp} \approx 1.00 \pm 0.05$ GeV. This comparison suggests that the QCD graphs reproduce the energy dependence of $\langle p_T \rangle$ very well, and it encourages more precise tests of the energy dependence predicted by the model, as illustrated in Figs. 15 and 17.

It is relevant to ask whether the value 1.04 GeV^2 is a reasonable amount of $\langle p_T^2 \rangle$ to assign to "confinement" effects. Apportioning it equally between the two initial constituents, I find that each constituent carries $\langle k_T^2 \rangle \approx 0.52$ GeV^2. This implies $\langle k_T \rangle \approx 600$ MeV per constituent, similar to the value which I suggested earlier should be provided by the fermi motion of quarks within a hadron. The value 600 MeV is also approximately the mean transverse momentum of ρ mesons and of "clusters" produced in inclusive hadronic reactions.[29] Finally, it is approximately the amount of internal transverse momentum which is assigned to the constituents in attempts to fit details of high p_T hadronic data.[26] In view of these arguments, the value of $\langle p_T^2 \rangle_{confinement} \approx 1.04$ GeV^2 does not seem too large.

Although I have discussed moments at some length, I believe that they do not provide a sensible test of QCD perturbation calculations. The answers in both the data and model calculations are much too influenced by the non-perturbative region

where $p_T < p_{T,crit} \simeq 1$ GeV. If one is in need of a single parameter for confronting theory with experiment, then perhaps it is best to fit $d\sigma/dM^2dydp_T^2$ to a simple form, say $\exp(-\lambda p_T)$, for $p_T > p_{T,crit}$, and to discuss the dependence of the slope λ on M, s, y, and x_F. I would be glad to supply interested readers with relevant predictions.

8. Antiproton Reactions. The reaction $\bar{p}p \to \ell^+\ell^- X$ serves in many respects as the cleanest test of the classical Drell-Yan mechanism. At large M, the cross-section is dominated by valence-valence annihilation, and it therefore measures the valence quark distribution almost directly. Shown in Fig.20 are the scaling cross-sections I compute with my structure functions for both $\bar{p}p \to \ell^+\ell^- X$ and $pp \to \ell^+\ell^- X$. The computation of the transverse momentum distribution of the lepton pairs produced in $\bar{p}N$ reactions proceeds along the same lines as for pN processes. In Fig.21, I present the first order QCD (Compton plus annihilation) contribution to $\langle p_T^2 \rangle$ for $\bar{p}N \to \mu\bar{\mu}X$ at 400 GeV/c and $y = 0$. In the $\bar{p}N$ case, the annihilation process $q\bar{q} \to G\mu\bar{\mu}$ dominates, and the Compton process $qG \to q\mu\bar{\mu}$ contributes a negligible portion of $\langle p_T^2 \rangle_{QCD}$. This situation may be contrasted with the pN case in Fig.16 where Compton and annihilation contributions are comparable. The results in Fig.21 suggest that transverse momentum effects in $\bar{p}N$ reactions are almost totally insensitive to the gluonic distribution. This provides another argument for the study of lepton pair production in antiproton collisions. Both the integrated cross-section and the transverse momentum distributions are controlled by valence-valence

annihilation diagrams.

The magnitude of $\langle p_T^2 \rangle_{QCD}$ for $\bar{p}N$ reactions is comparable to that of $\langle p_T^2 \rangle$ for pN collisions (c.f. Figs.16 and 21). I have not been able to trace the source of speculations that QCD predicts otherwise. In my results, $\langle p_T^2 \rangle_{QCD}^{\bar{p}N} > \langle p_T^2 \rangle_{QCD}^{pN}$ for $M < 9$ GeV. Above $M > 9$ GeV, $\langle p_T^2 \rangle^{pN}$ becomes larger, but this latter effect is sensitive to the choice of the gluon distribution. In attempting predictions for $\bar{p}N$ data, one must add a confinement contribution to the results of Fig.21. Since the confinement portion of $\langle p_T^2 \rangle$ is not "understood", I have no reason to believe that the same value of 1.04 GeV^2 deduced from the pN data should apply also in the $\bar{p}N$ case.

Just as in other branches of strong interaction phenomenology the chance to compare results from pN and $\bar{p}N$ processes in lepton pair production would aid our theoretical understanding considerably.

9. Dependence on x_F. In Fig.22 I present the calculated variation of $\langle p_T^2 \rangle_{QCD}$ expected when the longitudinal momentum x_F of the lepton pair is varied. Results are shown for both $\bar{p}N \to \mu\bar{\mu}X$ and $pN \to \mu\bar{\mu}X$ at 400 GeV/c and $M = 5$ GeV. In the pN case the Compton and annihilation contributions are about equal for the values of x_F shown; this breakdown is not presented here. To compare the predictions in Fig.22 with data, one must add a contribution for the confinement effects. This was found to be 1.04 GeV^2 in pN collisions at $x_F = 0$. The observation[1] that $\langle p_T^2 \rangle$ seems to be independent of x_F in the narrow range of available accept-

ance $0 < x_F < 0.2$ in pN collisions suggests that the confinement contribution may rise slightly with increasing x_F. However, here again, I stress that $\langle p_T^2 \rangle$ is not a suitable variable for tests of QCD. This objection is especially relevant when the calculated values of $\langle p_T \rangle_{QCD} \lesssim 1$ GeV. The entire answer is dominated by values of $p_T < p_{T,crit} \approx 1$ GeV where the perturbative calculation should not be used. It would be best to compare data directly with calculations of $d\sigma/dM^2 dx_F dp_T^2$ for values of $p_T > p_{T,crit}$.

10. <u>πN Collisions</u>. A wealth of data will soon be available on lepton pair production in $\pi^{\pm}N$ reactions.[2] Once the structure functions $q(x)$ and $\bar{q}(x)$ appropriate for the pion are deduced from these data, predictions for the transverse momentum spectra will follow readily.

VI. IMPLICATIONS AND CONCLUSIONS

Observation of the intermediate vector bosons, $W^{\pm}$ and Z^0, the mediators of weak interactions is one goal of high energy experimentation which seems almost within reach. The classical Drell-Yan mechanism has been used to provide estimates for W and Z^0 yields.[30] New structure functions deduced from the most recent data[1] on $pN \to \mu\bar{\mu}X$ and scaling violations[7-9] modify these predictions somewhat. However, the rather large values predicted by QCD for $\langle p_T \rangle_W$ would seem to have the most substantial impact on the design of experiments. Values of the slope b shown in Fig. 18 can be used to provide the expected values of $\langle p_T^2 \rangle_W$ at energies at which ISABELLE or the FNAL collider may operate. For example, for pp collisions of 400 GeV/c on 400 GeV/c ($\sqrt{s} = 800$ GeV), and for $M_W = 60$ GeV ($M_W/\sqrt{s} = 0.075$), $b = 0.575 \times 10^{-3}$. Consequently, $\langle p_T^2 \rangle_W \approx 368$ GeV^2, and $\langle p_T \rangle_W \approx 17$ GeV. At energies of the proposed CERN $\bar{p}p$ collider,[31,32] $\sqrt{s} = 2 \times 270$ GeV, with $M_W/\sqrt{s} \approx 0.11$, I calculate $b_{pp} = 0.79 \times 10^{-3}$ GeV^{-2}, and $b_{\bar{p}p} = 0.89 \times 10^{-3}$ GeV^{-2}. Therefore, I predict

$$\langle p_T^2 \rangle_{W,pp} \approx 230 \text{ GeV}^2,$$

and

$$\langle p_T \rangle_{W,pp} \approx 13 \text{ GeV}.$$

Likewise,

$$\langle p_T^2 \rangle_{W,\bar{p}p} \approx 260 \text{ GeV},$$

and

$$\langle p_T \rangle_{W,\bar{p}p} \approx 14 \text{ GeV}.$$

Obviously a considerable extrapolation has been made in energy to obtain these QCD predictions. The only basis for confidence in them is the fact the theory appears to reproduce data on $\langle p_T \rangle$ in the Fermilab energy range of 200 to 400 GeV/c. Restoration of the $\log(M^2/\Lambda^2)$ factor which I neglected after Eq. (16) would reduce my estimates slightly. On the other hand, experience with the Υ suggests that resonances are produced with larger $\langle p_T \rangle$ than the neighboring continuum.

A favored method for observing the W is to detect a sharp peak at $M_W/2$ in the single μ inclusive momentum spectrum. The peak signals the decay $W \to \mu\nu$. Once $\langle p_T \rangle_W$ exceeds ~10 GeV as I predict, this expected peak is substantially washed out, and other more difficult experimental methods to establish the W may have to be employed.[31,32]

There are many questions I have not addressed in this report which are nevertheless of considerable interest. Predictions have been made for various properties of the hadrons produced in association with a massive lepton pair.[33] The successful use of quark and antiquark distribution functions to explain the x dependence of the inclusive hadron yield $Ed\sigma/d^3p$ at small p_T also deserves further study.[34] Polarization phenomena[35] in constituent scattering processes may yield new insight into the dynamics of quarks and gluons.

Massive lepton pair production has become an industry on its own. It provides tests of several important aspects of the parton model of interacting quarks and gluons. Now that the

scaling predicted by the classical Drell-Yan model seems verified in the data, it is time to identify the scaling violations predicted by QCD. The process $pN \to \mu\bar{\mu}X$ serves to specify the average sea quark distribution in a region of Q^2 much higher than reached so far in inelastic neutrino reactions $\nu N \to \mu X$. To the extent that one accepts a QCD analysis of $\langle p_T^2 \rangle$ in $pN \to \mu\bar{\mu}X$, the average gluon distribution is also determined by this reaction. In Sec. V, I described in some detail the QCD approach for explaining the transverse momentum distribution of lepton pairs. The data from Fermilab on $\langle p_T^2 \rangle$ can be accommodated in a QCD calculation if we add an energy independent "confinement" contribution of 1.04 GeV^2 to the perturbative QCD prediction. It is desirable to understand this non-perturbative confinement portion in more detail. I mentioned a few important tests of the QCD calculation. In rough order of importance, I suggest:

1) verify the energy dependence predicted in Fig.15;
2) extend the data in Fig.14 to higher p_T to see whether theory and data diverge or converge;
3) obtain high statistics data on $\langle p_T \rangle$ and $\langle p_T^2 \rangle$ at ISR energies;
4) verify the energy dependence displayed in Fig.17;
5) obtain data on $\bar{p}N \to \mu\bar{\mu}X$; and
6) understand the x_F dependence of the p_T distribution, both the confinement and QCD portions.

ACKNOWLEDGMENTS

In preparing this report, I have benefited especially from discussions with S. Wolfram and M. Jacob. I acknowledge valuable conversations with J. Babcock, L. DiLella, J. Ellis, R. Petronzio, C. Sachrajda, J. C. Sens and T. M. Yan. I thank D. Sivers and G. Thomas for comments on the text. Some of the research I report here was done while I was a Visiting Scientist in the Theory Division at CERN. I am grateful to Jacques Prentki and others in the Division for their hospitality. This work was supported in part by the United States Department of Energy.

TABLE 1

A. Field and Feynman Model

$$xf(x) = g(x)\sum_{k=0}^{N}(a_k + \sqrt{x}b_k)C_k(x)$$

$$C_k(x) = \cos\left(k\cos^{-1}(2x-1)\right)$$

xf(x)	xu(x)	xd(x)	xs(x)	$x\bar{u}(x)$	$x\bar{d}(x)$	$x\bar{s}(x)$
g(x)	$(1-x)^3$	$(1-x)^4$	$(1-x)^8$	$(1-x)^{10}$	$(1-x)^7$	$(1-x)^8$
a_0	161.579	-3.175	0.10	0.17	0.17	0.10
a_1	225.327	-2.937	0.0	0.0	0.0	0.0
a_2	70.699	1.082	0.0	0.0	0.0	0.0
a_3	6.761	0.674	0.0	0.0	0.0	0.0
b_0	-177.909	5.607	0.0	0.0	0.0	0.0
b_1	-230.510	2.6340	0.0	0.0	0.0	0.0
b_2	-52.427	-2.288	0.0	0.0	0.0	0.0
b_3	-1.371	-0.247	0.0	0.0	0.0	0.0

B. Hybrid Model

Derived from the Field-Feynman Model by the substitutions(for each species: u,d,s)

$$x\bar{q}(x) = 0.42(1-x)^9$$

$$xq(x) = xq_{FF}(x) - x\bar{q}_{FF}(x) + 0.42(1-x)^9$$

REFERENCES

1. Columbia-Fermilab-Stony Brook Collaboration, R. Kephart, Proceedings of the 3rd International Conference at Vanderbilt University on New Results in High Energy Physics.
2. Chicago-Princeton Collaboration, K. J. Anderson, ibid.
3. S. D. Drell and T. M. Yan, Phys. Rev. Lett. 25, 316 (1970); Ann. Phys. (N.Y.) 66, 578 (1971). For a recent discussion of the subject, consult the review by T. M. Yan, presented at the VIII International Symposium on Multiparticle Dynamics, Kaysersberg, France, June, 1977.
4. D. Antreasyan et al Phys. Rev. Lett. 39, 906 (1977).
5. J. H. Cobb et al, Phys. Lett. 72B, 273 (1977).
6. D. M. Kaplan et al, Phys. Rev. Lett. 40, 435 (1978).
7. I. Hinchliffe and C. H. Llewellyn Smith, Phys. Lett. 66B, 281 (1977) and Nucl. Phys. B128, 93 (1977).
8. N. Cabibbo and R. Petronzio, CERN report Ref. TH. 2440 (1978).
9. J. Kogut and J. Shigemitsu, Nucl. Phys. B129, 461 (1977).
10. A goldmine of information on the past, present, and future of experiments on lepton pair production at Fermilab, CERN-SPS, and CERN-ISR energies is the CERN report ISR Workshop/ 2-8 (October, 1977), edited by M. Jacob. For a review of the experimental situation as of the Summer of 1977, consult the paper by M. J. Shochet, Univ. of Chicago report EFI 77-66, presented at the SLAC Summer Institute, July, 1977.
11. M. Duong-Van, SLAC report, SLAC-Pub-1819 (1976); J. Gunion, Phys. Rev. D14, 1400 (1976); F. Close, F. Halzen, and D. Scott, Phys. Lett. 68B, 447 (1977); A. Davis and E. J. Squires,

Phys. Lett. 69B, 249 (1977); J. Bell and A.J.G. Hey, CERN report Ref.TH-2437 (1977); and R. C. Hwa, S. Matsuda, and R. G. Roberts CERN report Ref. TH-2456 (1978).

12. M. Duong-Van, K. V. Vasavada, and R. Blankenbecler, Phys. Rev. D16, 1389 (1977); M. Duong-Van and R. Blankenbecler, SLAC-Pub-2017 (Sept. 1977).

13. C. S. Lam and T. M. Yan, Phys. Lett. 71B, 173 (1977); J. Kogut and J. Shigemitsu, Phys. Lett. 71B, 165 (1977) H. D. Politzer, Nucl. Phys. B129, 301 (1977); H. Fritzsch and P. Minkowski Phys. Lett. 73B, 80 (1978); G. Altarelli, G. Parisi, and R. Petronzio, CERN report Ref. TH. 2413 (October, 1977) and CERN report Ref. TH. 2450 (January, 1978); K. Kajantie and R. Raitio, Helsinki report HU-TFT-77-21 (October, 1977); F. Halzen and D. Scott, Univ. Wisconsin, Madison, report C00-881-21 (Feb., 1978); K. Kajantie, J. Lindfors, and R. Raitio, Helsinki report HU-TFT-78-5 (1978).

14. E. L. Berger, J. Donohue, and S. Wolfram, Phys. Rev. D17, 858 (1978).

15. K. V. Vasavada, Phys. Rev. D16, 146 (1977).

16. J. C. Collins and D. E. Soper Phys. Rev. D16, 2219 (1977).

17. Gargamelle Neutrino Collaboration, H. Deden et al Nucl. Phys. B85, 269 (1975).

18. R. D. Field and R. P. Feynman, Phys. Rev. D16, 2590 (1977).

19. I have not made a survey of all the different models for structure functions. A partial list of references includes P. V. Landshoff and J. C. Polkinghorne, Nucl. Phys. B33, 221 (1971); R. McElhaney and S. F. Tuan, Phys. Rev. D8, 2267 (1973); G. Farrar, Nucl. Phys. B77, 429 (1974); V. Barger

and R.J.N. Phillips, Phys. Lett. 73B, 91 (1978); and F. T. Dao et al Phys. Rev. Lett. 39, 1388 (1977).

20. BEBC Neutrino collaborations, J. Mulvey, these proceedings.

21. H. L. Anderson et al, Phys. Rev. Lett. 38, 1450 (1977).

22. S. M. Berman, D. J. Levy, and T. L. Neff Phys. Rev. Lett. 23, 1363 (1969).

23. H. D. Politzer, Rev. 13; C. T. Sachrajda, Phys. Lett. B73, 185 (1978); J. B. Kogut, Phys. Lett 65B, 377 (1976); H. Georgi, Harvard report HUTP-78/A003 (1978 Orbis Scientiae, Coral Gables, Florida). K. H. Craig and C. H. Llewellyn Smith Oxford report TP 67/77 (Nov. 1977).

24. Consult, e.g., A. DeRujula, H. Georgi, and H. D. Politzer, Ann. Phys. (N.Y.) 103, 315 (1977); G. C. Fox, Nucl. Phys. B131, 107 (1977). I. Hinchliffe and C. H. Llewellyn Smith, Ref.7; A. J. Buras and K.J.F. Gaemers, CERN report Ref. TH-2322 (1977); G. Altarelli and G. Parisi, Nucl. Phys. B126, 298 (1977); C. H. Llewellyn Smith and S. Wolfram, Oxford report 6/78 (1978).

25. I am grateful to J. Babcock for help in the derivation of Eqs.(20) and (21). See also some of the papers listed in Ref.13.

26. R. P. Feynman, R. D. Field, and G. C. Fox, Nucl. Phys. B128, 1 (1977).

27. H. Georgi and M. Machacek, Phys. Rev. Lett. 39, 1237, (1977); E. Farhi, Phys. Rev. Lett. 39, 1587, (1977); and A. DeRujula, J. Ellis, E. G. Floratos, and M. K. Gaillard, CERN report Ref. TH 2455 (1978).

28. G. Sterman and S. Weinberg, Phys. Rev. Lett. 39, 1436 (1977).

29. D. R. O. Morrison, Review presented at the Symposium on Hadron Structure and Multiparticle Production, Kazimierz, Poland, May, 1977 CERN EP report (1977); and CERN-College de France-Heidelberg-Karlsruhe Collaboration, M. Della Negra et. al., CERN report CERN/EP/PHYS-77-30 (1977).

30. C. Quigg, Rev. Mod. Phys. 49, 297 (1977); R. F. Peierls, T. L. Trueman, and L. L. Wang, Phys. Rev. D16, 1397 (1977).

31. Aachen-Annecy-Birmingham-CERN-College de France-Queen Mary-Riverside-Rutherford-Saclay Collaboration Proposal, A. Astbury et. al, CERN/SPSC/78-06 (1978).

32. Saclay-CERN-Orsay Proposal, M. Banner et. al., CERN/SPSC/78-8 (1978).

33. T. A. DeGrand and H.I. Miettinen, Phys. Rev. Lett. 40, 612 (1978).

34. W. Ochs, Nucl. Phys. B118, 397 (1977); K. P. Das and R. C. Hwa, Phys. Lett. 68B, 459 (1977); F. C. Erné and J. C. Sens, CERN report, 1978, submitted to Phys. Rev. Letters.

35. F. Close and D. Sivers, Phys. Rev. Letters, 39, 1116 (1977); J. Babcock, E. Monsay, and D. Sivers, Argonne report ANL-HEP-PR-78-07.

FIGURE CAPTIONS

1. Basic Drell-Yan quark-antiquark annihilation mechanism for lepton pair production in hadronic collisions, illustrated here for $h_1 h_2 \to \mu\bar{\mu}X$; q and $\bar{q}$ denote respectively a quark and an antiquark constituent.
2. ISR data from Ref.5 are compared with a scaling curve obtained from the hybrid model described in Section III.6. The model is constructed to fit lepton pair data at $p_{lab} = 400$ GeV/c, $y = 0$, and $0.2 < M/\sqrt{s} < 0.5$.
3. The first two moments (a) $\langle p_T \rangle$ and (b) $\langle p_T^2 \rangle$ of the transverse momentum distribution of muon pairs produced in $pp \to (\mu\bar{\mu})X$ at 400 GeV/c and $y = 0$ are shown as a function of the mass of the muon pair. The data are from Ref.6. The theoretical curves are calculated from simple models in which the initial quarks and antiquarks are assigned a distribution in their transverse momenta. The two models (Gaussian and exponential) are described in the text.
4. (a) Diagram which illustrates the scattering of a quark and a gluon constituent to produce a lepton pair and a quark (which, in turn, fragments into a jet of hadrons). (b) Quark-antiquark scattering to produce a lepton pair and a gluon jet.
5. The inclusive yield of muon pairs $Ed\sigma/d^3p$ shown as a function of p_T for $5 < M_{\mu\mu} < 6$ GeV, at $y = 0$ and 400 GeV/c. The data are from Ref.6. The theoretical curves are obtained from simple models in which the initial quarks and antiquarks in the hadrons are assigned a distribution in their transverse momenta k_T. In one model, this distribution is chosen

to be an exponential in $|k_T|$ with $\langle |k_T| \rangle = 0.8$ GeV; in the other, a Gaussian is chosen with $\langle |k_T| \rangle = 0.86$ GeV. The p_T distribution in the data at other values of mass (not shown) is also described equally well with these models.

6. Predicted p_T dependence of the coefficient α_t in the t channel angular distribution $d\sigma/d\Omega \propto [1 + \alpha_t \cos\theta_t]$ for lepton pairs of mass $M = 5.5$ GeV produced in $pN \to \ell^+\ell^- X$ at 400 GeV/c and $y = 0$; p_T is the transverse momentum of the $\ell^+\ell^-$ pair. The two models used are described in the text.

7. Cross-section $d^2\sigma/dMdy$ for $pN \to \mu\bar{\mu}X$ at 400 GeV/c and $y = 0$ shown as a function of the lepton pair mass M. The data are from Ref.6. The dashed curve is obtained from the Field-Feynman structure functions, Ref.18. In the calculation, N = 60% protons and 40% neutrons. The solid curve is a fit to the data obtained from the hybrid model described in the text.

8. First order processes in the strong coupling constant α_s. Diagrams (a) and (b) represent quark-gluon Compton scattering to yield a quark and a virtual photon. Diagrams (c) and (d) represent quark-antiquark annihilation into a gluon and a virtual photon.

9. Some second order processes which contribute to the production of massive virtual photons.

10. Diagrams in deep inelastic electron scattering.

    a) Classical quark model diagram in which an exchanged photon scatters from a quark constituent in the hadron N.

b) The first order contribution in which $\gamma q \to qG$, where G is a gluon.

c) The first order contribution in which the exchanged photon scatters from a gluon in the target to yield quark and antiquark systems in the final state.

11. The x dependence of the gluon and sea parton distributions in a proton expected for different values of Q^2 according to QCD. This figure is adapted from Hinchliffe and Llewellyn Smith, Ref.7, with the scale parameter $\Lambda^2 = 0.5$ GeV^2.

12. In part (a), the process is shown in which $h_1 h_2 \to \mu\bar{\mu}X$ via the constituent scattering process $q\bar{q} \to \gamma G$. The transverse momentum of the γ is balanced by a gluon jet. In (b) the c.of.m. distribution of particles is shown in the final state. The dashed line indicates the longitudinal axis of the original collision. The forward and backward jets represent debris from the incident hadrons h_1 and h_2. A jet of hadrons from the gluon dissociation is roughly back-to-back with the virtual photon.

13. ISR and Fermilab data on $\langle p_T \rangle$ are shown as a function of lab momentum. The FNAL data (from Ref.1) are from the reaction $pN \to \mu\bar{\mu}X$ and are an average over the range $0.2 < M/\sqrt{s} < 0.4$. The ISR data (Ref.5) are from $pp \to e^+e^-X$ and correspond to $M/\sqrt{s} \simeq 0.1$.

14. Data are shown from Ref.6 on the p_T distribution of $pN \to \mu\bar{\mu}X$ at 400 GeV/c and $y = 0$ in the dimuon mass interval $7 \leq M \leq 8$ GeV. Shown also are calculations of the QCD expectations for this distribution. The theoretical curves are obtained from an evaluation of Eqs.(27) and (28) of the text.

An integral was also performed over M to yield $Ed\sigma/d^3p$. The curves are normalized absolutely; $\alpha_s = 0.3$. The solid curve marked "total" is obtained from an incoherent addition of the Compton and annihilation contributions. Indicated by cross-hatching is the critical $p_T \simeq 1$ GeV below which the perturbation calculation is inapplicable, as discussed in Sec. V.5. The comparison of theory and experiment is similar for other values of M (not shown).

15. Theoretical results on the energy dependence expected if QCD processes dominate the reaction $pN \to \mu\bar{\mu}X$. Curves are presented for three values of lab momentum in the Fermilab and CERN-SPS energy range and for one ISR momentum value. At all energies, $\tau = M^2/s = 0.07$, and $x = 0$.

16. Shown are values of $\langle p_T^2 \rangle$ computed according to the definition given in Eqs. (44) and (46) of the text. The short dashed line illustrates the value obtained from the annihilation process $q\bar{q} \to G\mu\bar{\mu}$, and the long dashed line represents the contribution of the Compton process $qG \to q\mu\bar{\mu}$. The dotted line is the net QCD contribution to $\langle p_T^2 \rangle$ to first order in α_s; it is obtained by addition of the Compton and annihilation portions. The solid line is obtained from the "net QCD" curve by addition of the constant confinement contribution 1.04 GeV^2. The data are from Ref. 6. All curves are calculated for the process $pN \to \ell^+\ell^-X$ at $p_{lab} = 400$ GeV/c and $y = 0$. In this paper N is composed of 60% neutrons and 40% protons.

17. The first order (Compton plus annihilation) QCD contribution to $\langle p_T^2 \rangle$ is shown as a function of M for the process $pN \to \mu\bar{\mu}X$ at $y = 0$ for three values of lab momentum.

18. In the expression $\langle p_T^2 \rangle = a + bs$, the slope b computed from the first order QCD graphs is shown as a function of $M/\sqrt{s}$. These slopes can be used to obtain predictions for $\langle p_T^2 \rangle$ at various lab energies and lepton pair masses.

19. Shown are expectations for the mean transverse momentum $\langle p_T \rangle$ of lepton pairs produced in $pN \to \mu\bar{\mu}X$ at $y = 0$ and $p_{lab} = 200$ and 400 GeV/c. The curves are derived from Eqs. (47) and (49) of the text.

20. Estimates of the lepton pair yield in antiproton-proton collisions are presented as a function of $M/\sqrt{s}$ at $y = 0$ and are compared with yields in pp collisions.

21. A prediction of the first order QCD expectation for $\langle p_T^2 \rangle$ in antiproton-nucleon collisions at 400 GeV/c and $y = 0$ for various masses of the lepton pair. Shown also is the breakdown of the answer into the contributions from the Compton and annihilation processes shown in Fig. 4.

22. A prediction for the dependence of $\langle p_T^2 \rangle_{QCD}$ on the longitudinal momentum fraction x_F of the lepton pair in both pN and $\bar{p}N$ collisions at 400 GeV/c and at the lepton pair mass $M = 5$ GeV.

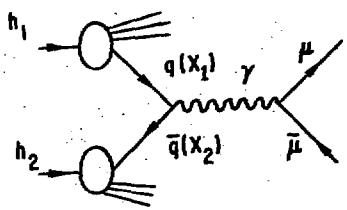

Fig. 1

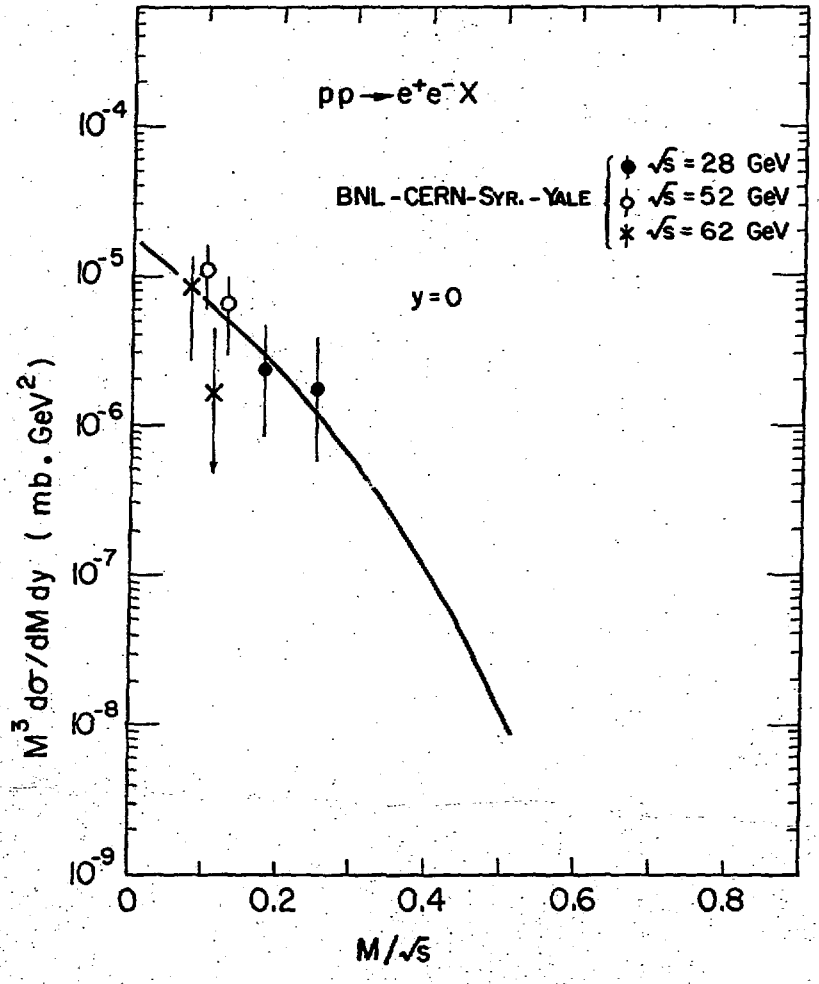
pp → e⁺e⁻X
BNL - CERN - SYR. - YALE
√s = 28 GeV
√s = 52 GeV
√s = 62 GeV
y = 0
M³ dσ/dM dy (mb . GeV²)
10⁻⁴
10⁻⁵
10⁻⁶
10⁻⁷
10⁻⁸
10⁻⁹
0
0.2
0.4
0.6
0.8
M/√s

Fig. 2

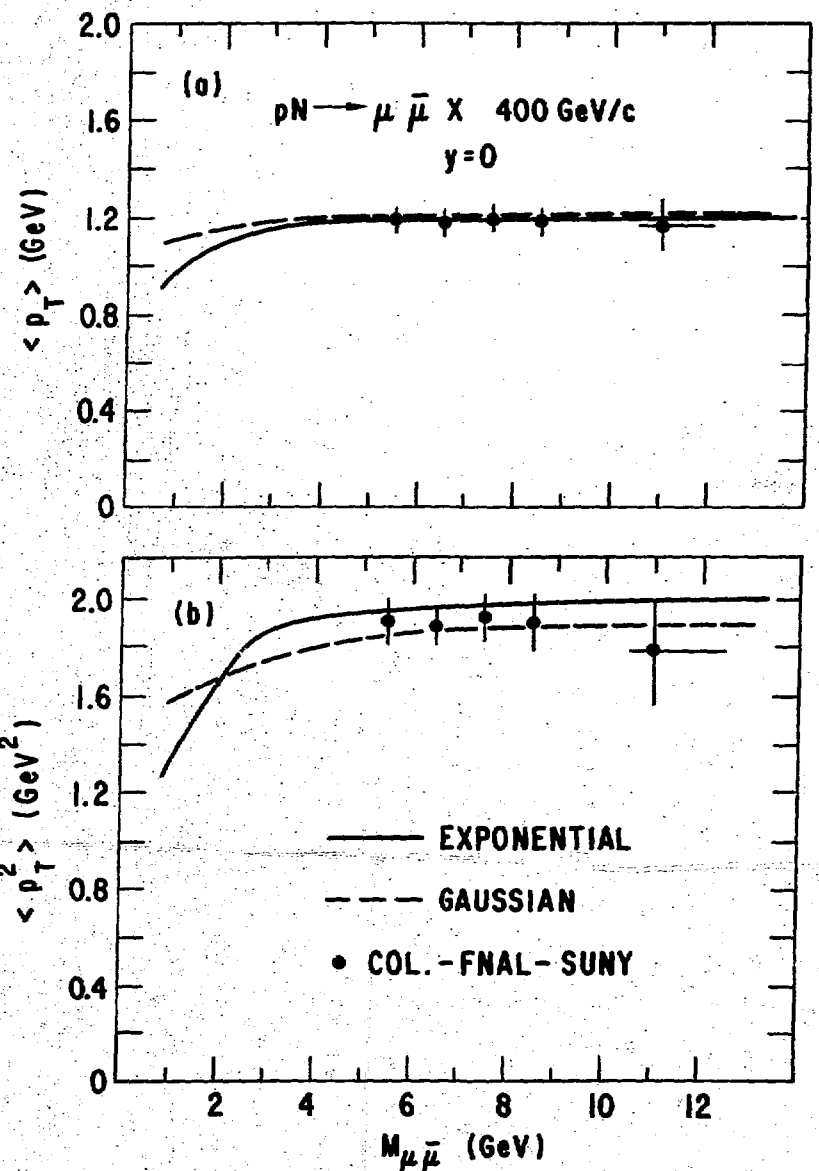
(a)
pN → μ μ̄ X 400 GeV/c
y=0
<p_T> (GeV)
2.0
1.6
1.2
0.8
0.4
0
(b)
<p_T^2> (GeV^2)
EXPONENTIAL
GAUSSIAN
COL.-FNAL-SUNY
2
4
6
8
10
12
M_μμ̄ (GeV)

Fig. 3

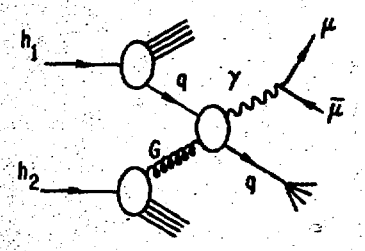

(a)

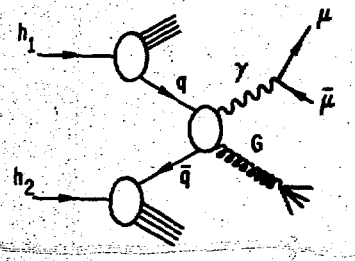

(b)

Fig. 4

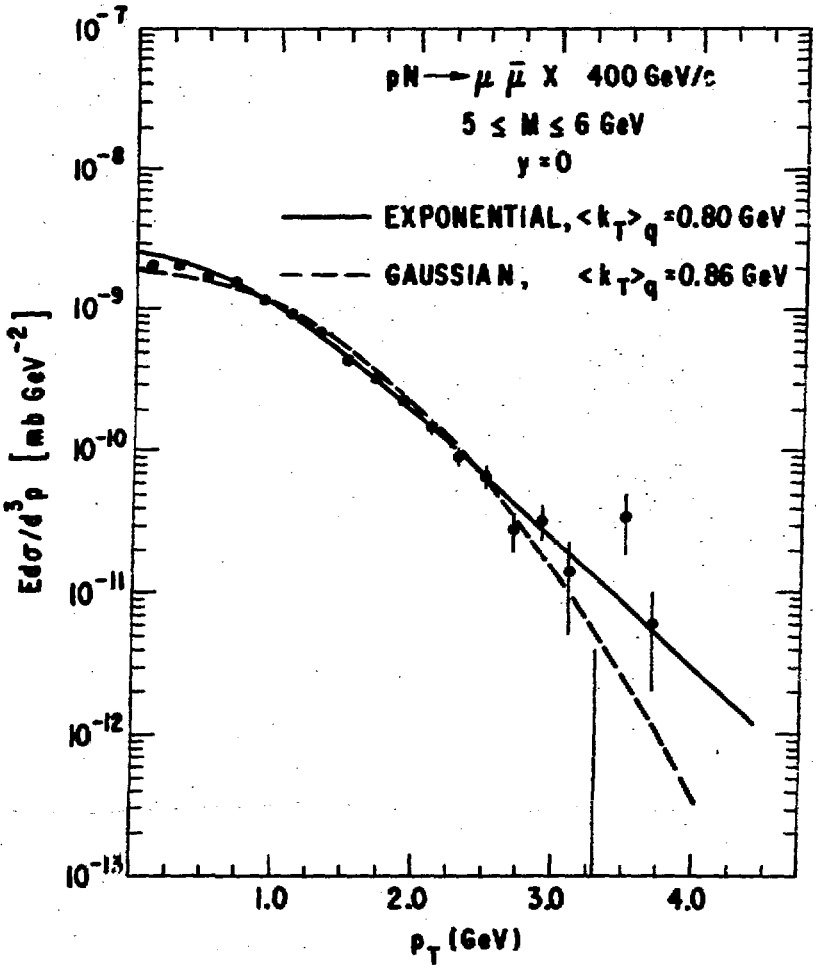
pN → μ μ̄ X 400 GeV/c
5 ≤ M ≤ 6 GeV
y = 0
EXPONENTIAL, <k_T>_q = 0.80 GeV
GAUSSIAN, <k_T>_q = 0.86 GeV
Edσ/d³p [mb GeV⁻²]
p_T (GeV)
10⁻⁷
10⁻⁸
10⁻⁹
10⁻¹⁰
10⁻¹¹
10⁻¹²
10⁻¹³
1.0
2.0
3.0
4.0

Fig. 5

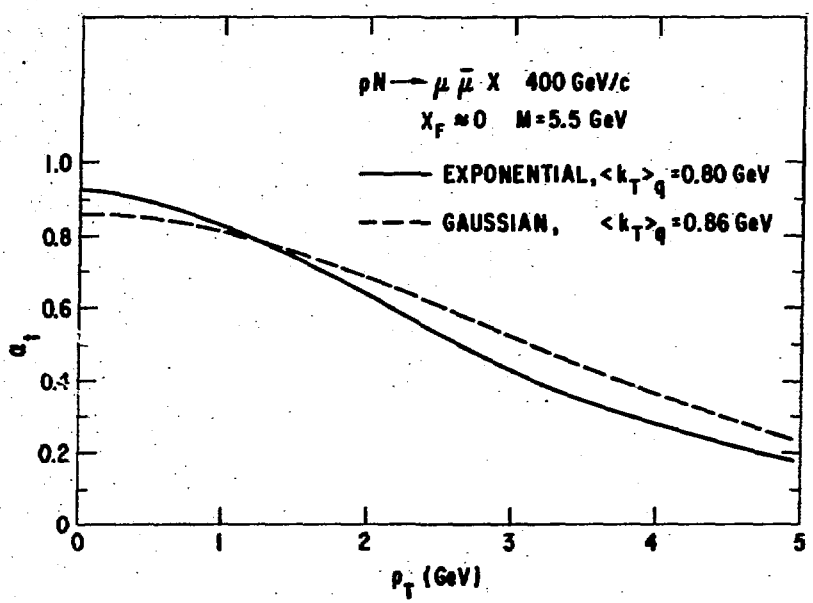
pN → μ μ̄ X 400 GeV/c
X_F ≈ 0 M = 5.5 GeV
EXPONENTIAL, <k_T>_q = 0.80 GeV
GAUSSIAN, <k_T>_q = 0.86 GeV
1.0
0.8
0.6
0.4
0.2
0
0
1
2
3
4
5
p_T (GeV)

Fig. 6

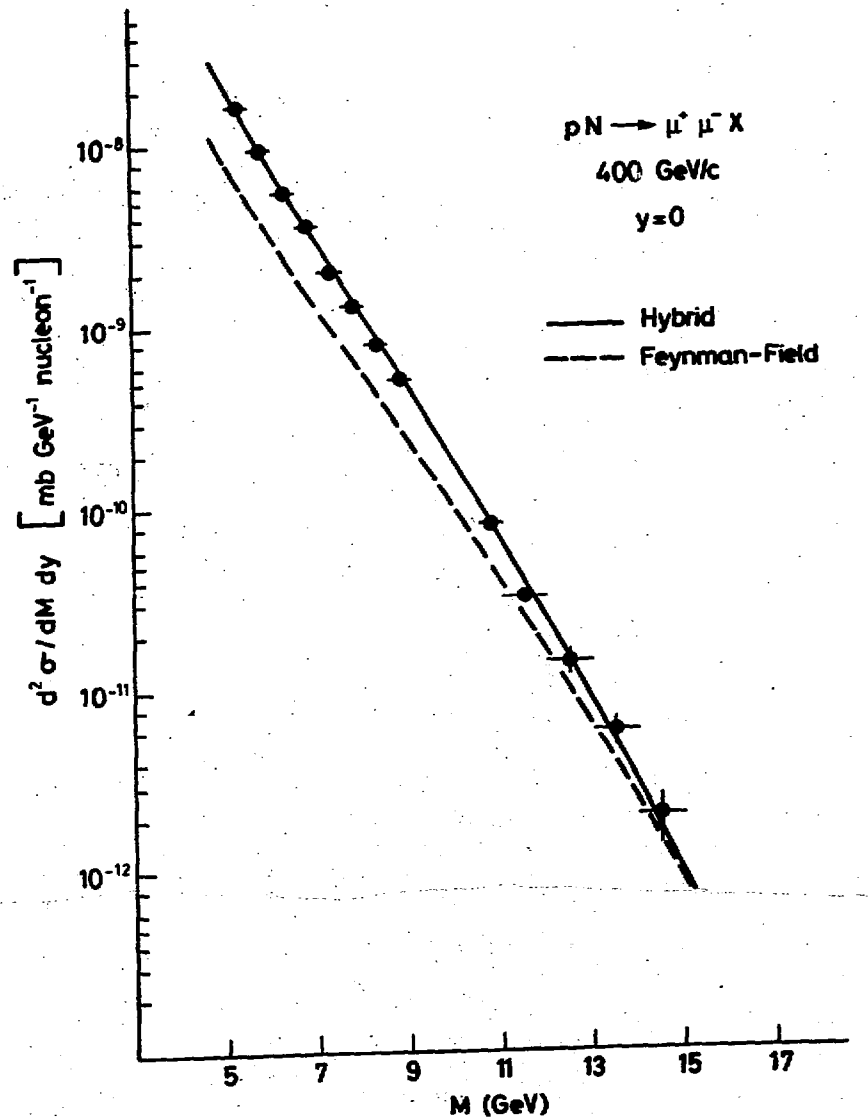
pN → μ⁺ μ⁻ X
400 GeV/c
y=0
Hybrid
Feynman-Field
d²σ/dM dy [mb GeV⁻¹ nucleon⁻¹]
10⁻⁸
10⁻⁹
10⁻¹⁰
10⁻¹¹
10⁻¹²
5
7
9
11
13
15
17
M (GeV)

Fig. 7

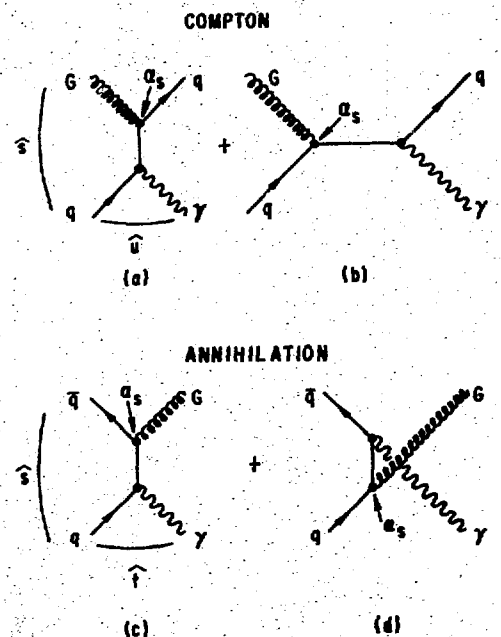
COMPTON
G
α_s
q
$\hat{s}$
q
γ
$\hat{u}$
(a)
+
G
α_s
q
q
γ
(b)
ANNIHILATION
$\bar{q}$
α_s
G
$\hat{s}$
q
γ
$\hat{t}$
(c)
+
$\bar{q}$
G
q
α_s
γ
(d)

Fig. 8

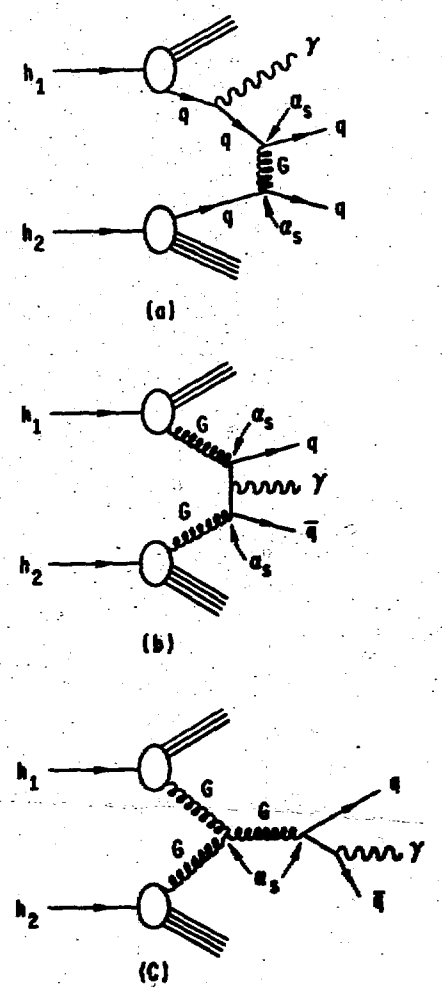

Fig. 9

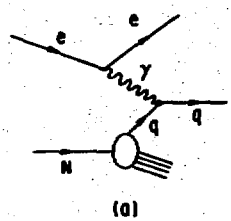

(a)

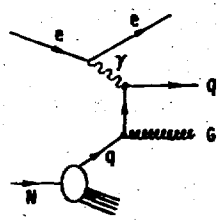

(b)

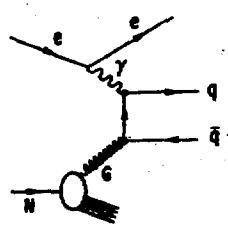

(c)

Fig. 10

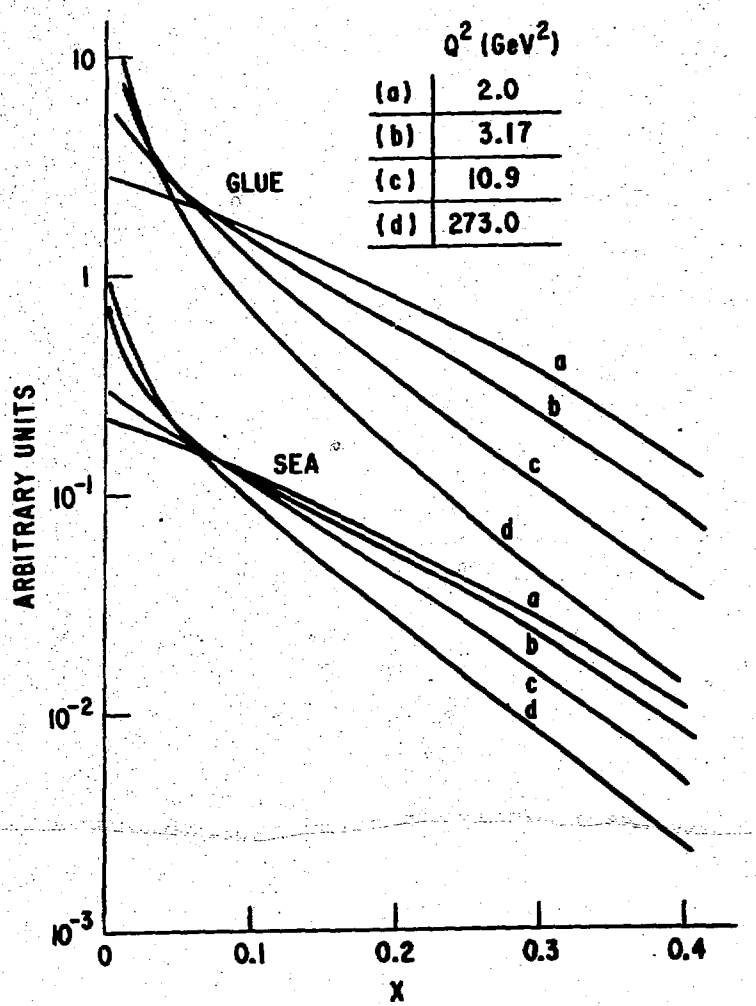
Q^2 (GeV^2)
(a) 2.0
(b) 3.17
(c) 10.9
(d) 273.0
GLUE
SEA
a
b
c
d
a
b
c
d
ARBITRARY UNITS
10
1
10^{-1}
10^{-2}
10^{-3}
0
0.1
0.2
0.3
0.4
X

Fig. 11

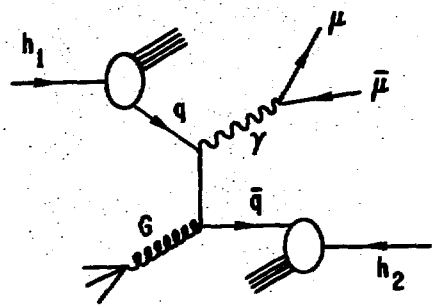

(a)

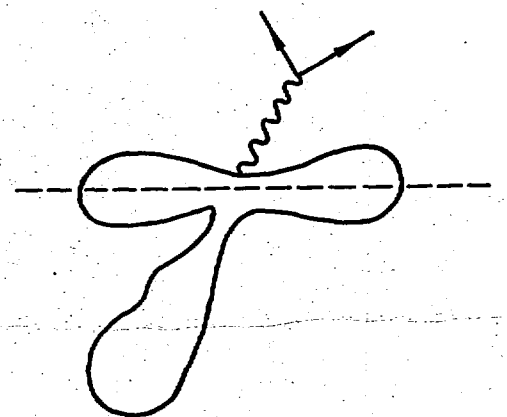

(b)

Fig. 12

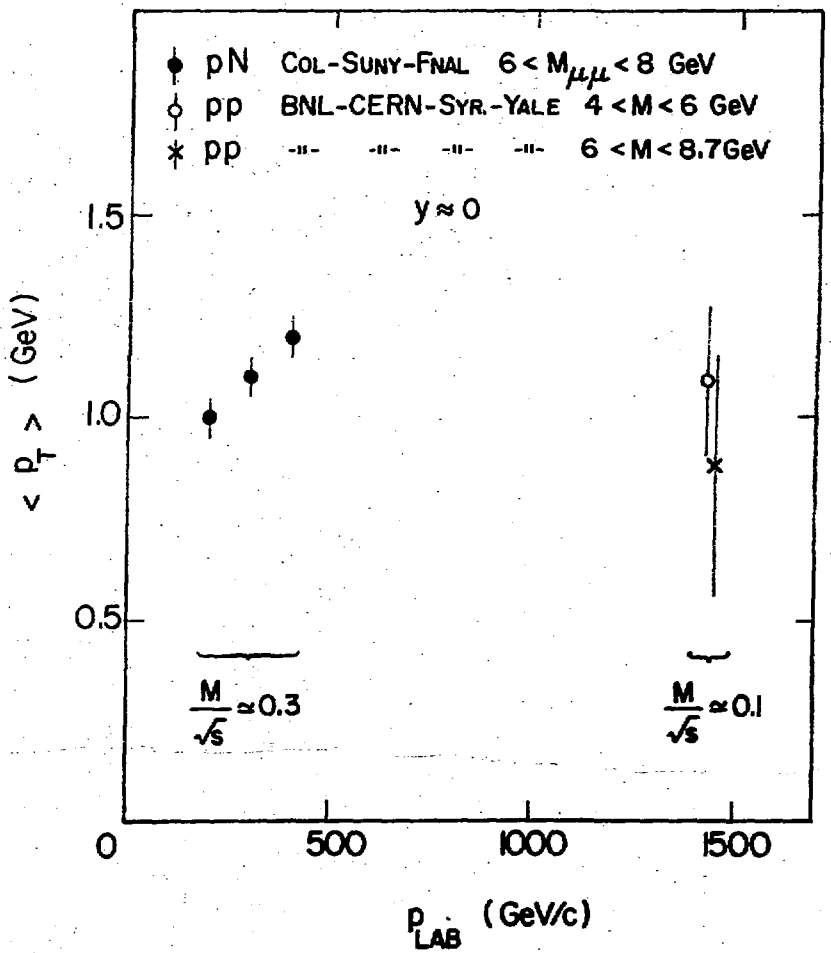
pN COL-SUNY-FNAL 6 < Mμμ < 8 GeV
pp BNL-CERN-SYR.-YALE 4 < M < 6 GeV
pp -"- -"- -"- -"- 6 < M < 8.7GeV
y ≈ 0
1.5
1.0
0.5
0
500
1000
1500
< pT > (GeV)
M/√s ≃ 0.3
M/√s ≃ 0.1
pLAB (GeV/c)

Fig. 13

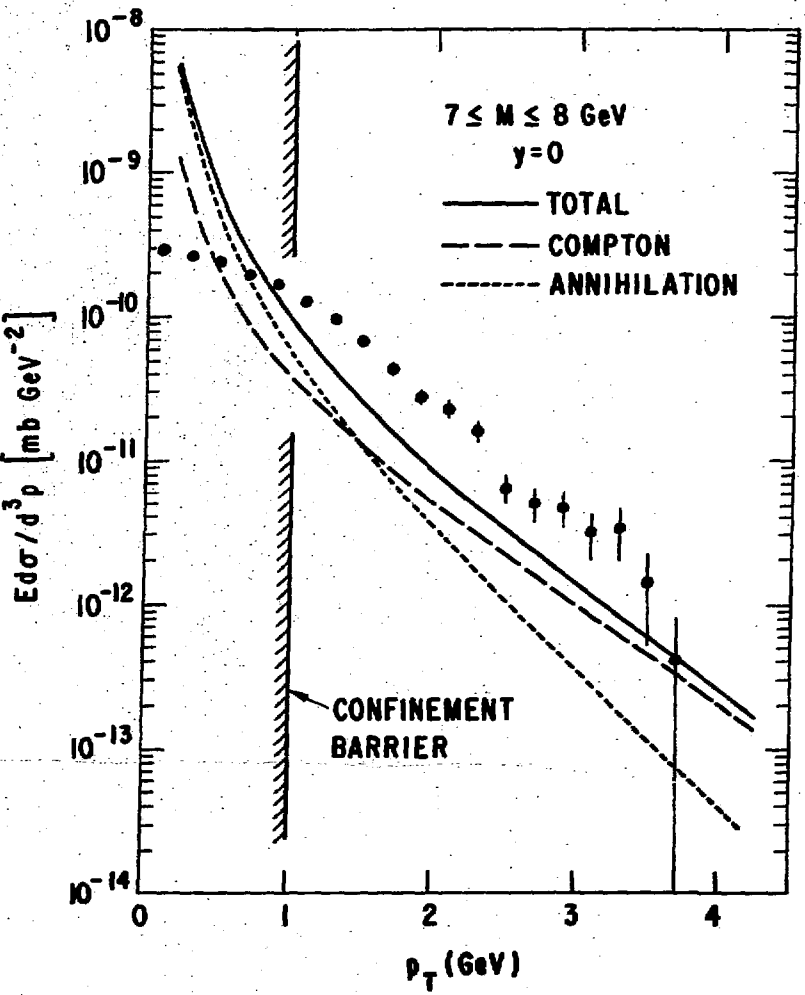
10^{-8}
10^{-9}
10^{-10}
10^{-11}
10^{-12}
10^{-13}
10^{-14}
$E d\sigma/d^3p$ [mb GeV^{-2}]
$7 \leq M \leq 8$ GeV
y=0
TOTAL
COMPTON
ANNIHILATION
CONFINEMENT
BARRIER
0
1
2
3
4
p_T (GeV)

Fig. 14

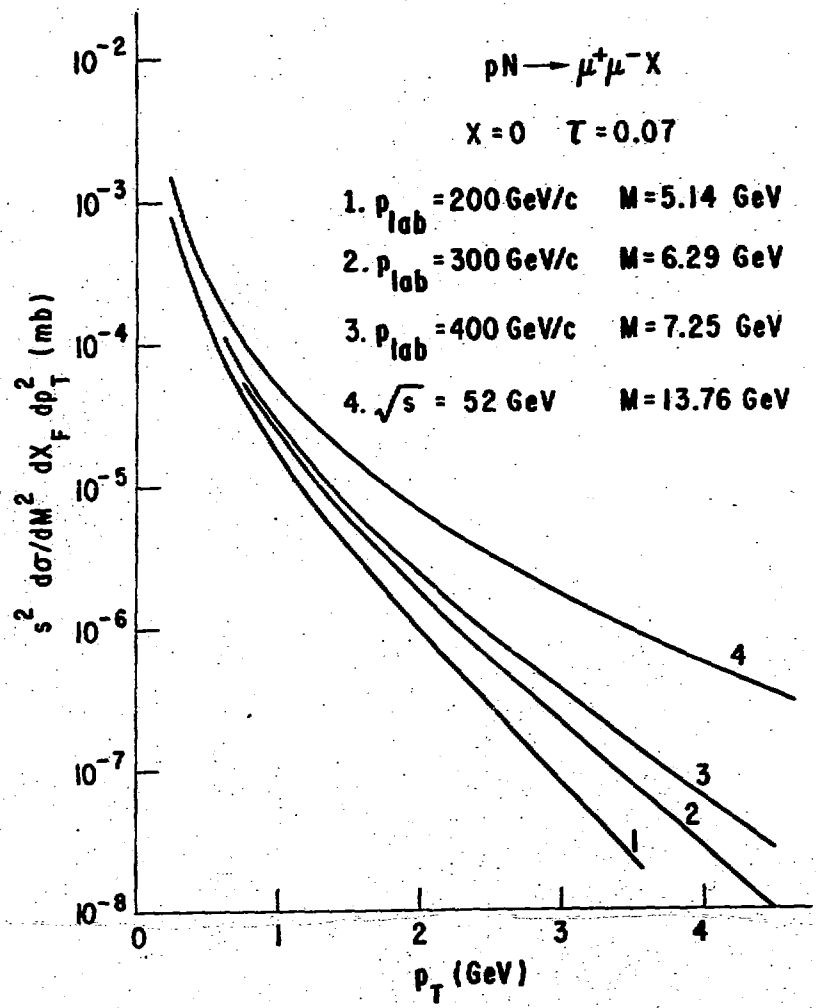
$pN \rightarrow \mu^+\mu^- X$
$X = 0 \quad \tau = 0.07$
1. p_{lab} = 200 GeV/c M = 5.14 GeV
2. p_{lab} = 300 GeV/c M = 6.29 GeV
3. p_{lab} = 400 GeV/c M = 7.25 GeV
4. $\sqrt{s}$ = 52 GeV M = 13.76 GeV
$s^2 \, d\sigma/dM^2 \, dX_F \, dp_T^2$ (mb)
10^{-2}
10^{-3}
10^{-4}
10^{-5}
10^{-6}
10^{-7}
10^{-8}
0
1
2
3
4
p_T (GeV)

Fig. 15

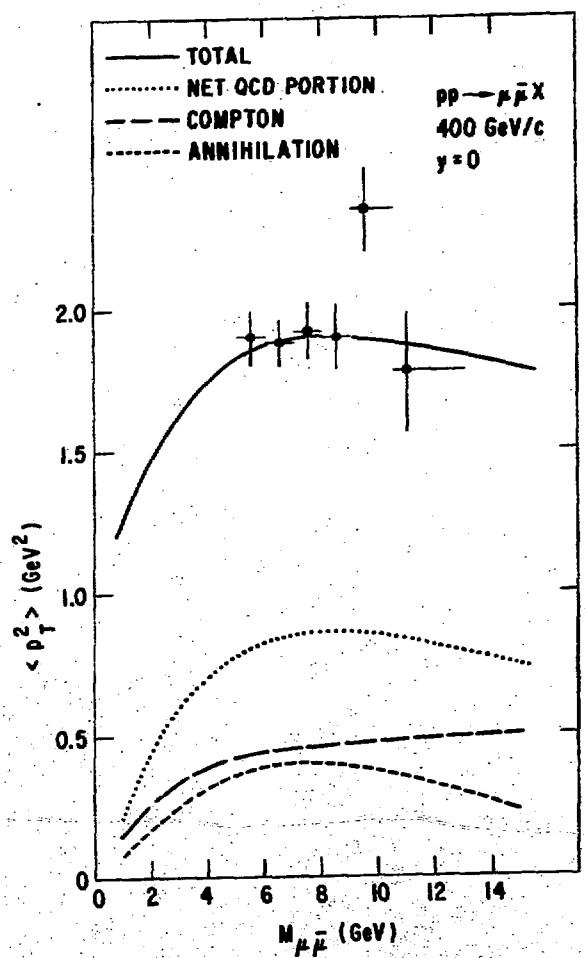
TOTAL
NET QCD PORTION
COMPTON
ANNIHILATION
pp → μμ̄X
400 GeV/c
y = 0
2.0
1.5
1.0
0.5
0
0
2
4
6
8
10
12
14
$\langle p_T^2 \rangle$ (GeV^2)
$M_{\mu\bar{\mu}}$ (GeV)

Fig. 16

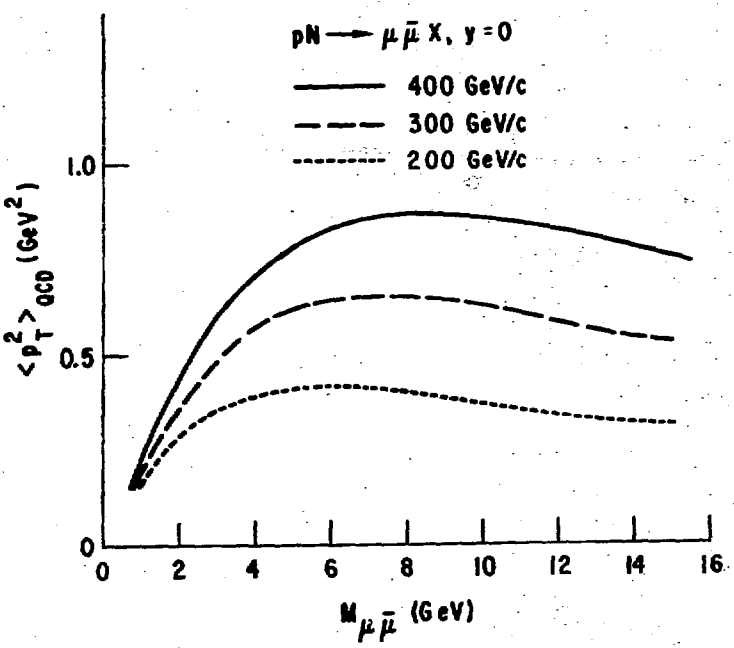
pN → μμ̄ X, y = 0
400 GeV/c
300 GeV/c
200 GeV/c
$\langle p_T^2 \rangle_{QCD}$ (GeV^2)
1.0
0.5
0
0
2
4
6
8
10
12
14
16
$M_{\mu\bar{\mu}}$ (GeV)

Fig. 17

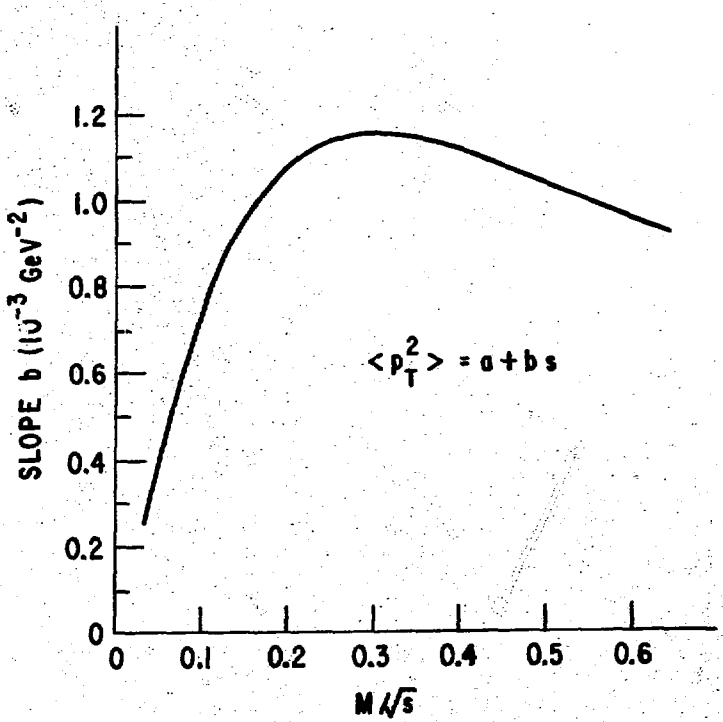
SLOPE b (10^{-3} GeV^{-2})
1.2
1.0
0.8
0.6
0.4
0.2
0
0
0.1
0.2
0.3
0.4
0.5
0.6
$M/\sqrt{s}$
$\langle p_T^2 \rangle = a + b\,s$

Fig. 18

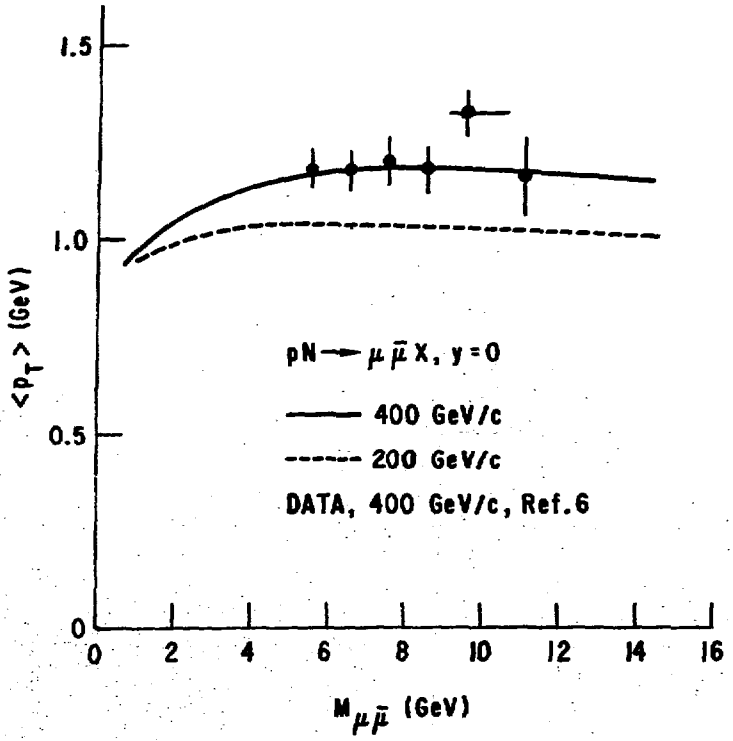
1.5
1.0
0.5
0
$\langle p_T \rangle$ (GeV)
$pN \rightarrow \mu\bar{\mu} X$, y = 0
400 GeV/c
200 GeV/c
DATA, 400 GeV/c, Ref.6
0
2
4
6
8
10
12
14
16
$M_{\mu\bar{\mu}}$ (GeV)

Fig. 19

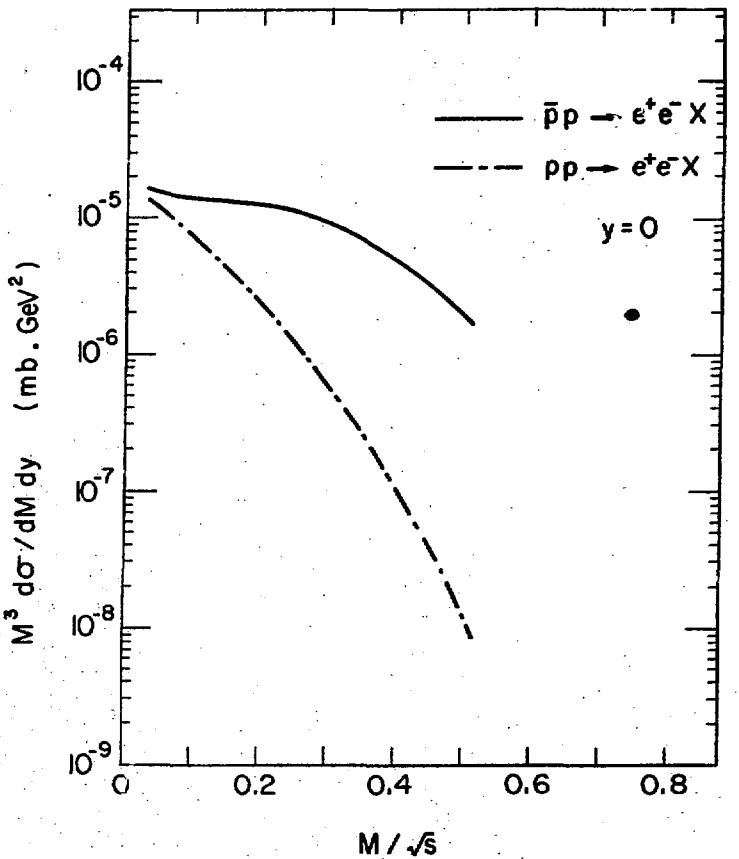
10^{-4}
10^{-5}
10^{-6}
10^{-7}
10^{-8}
10^{-9}
$M^3\, d\sigma/dM\, dy$ (mb. GeV^2)
$\bar{p}p \rightarrow e^+e^-X$
$pp \rightarrow e^+e^-X$
y = 0
0
0.2
0.4
0.6
0.8
$M/\sqrt{s}$

Fig. 20

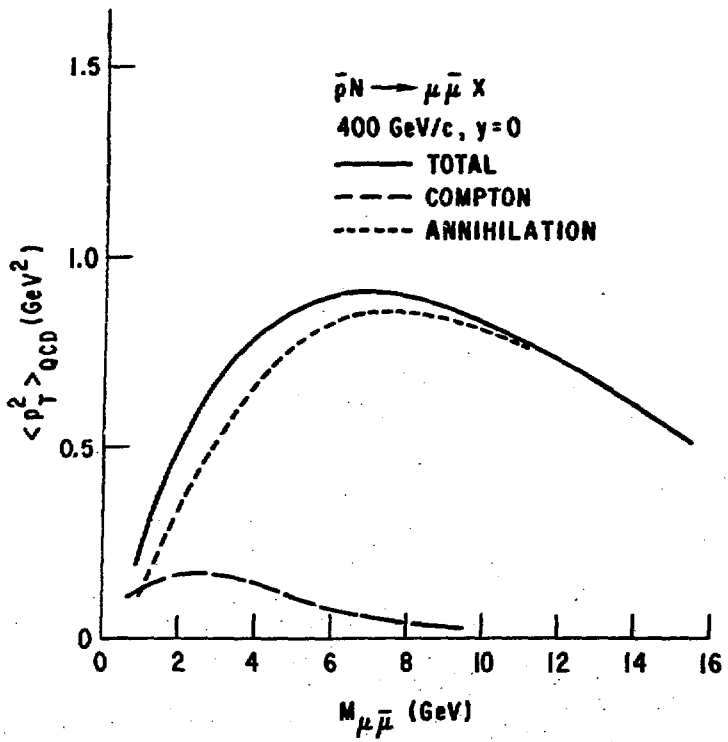
1.5
1.0
0.5
0
$\langle p_T^2 \rangle_{QCD}$ (GeV^2)
$\bar{p}N \rightarrow \mu\bar{\mu}\,X$
400 GeV/c, y=0
TOTAL
COMPTON
ANNIHILATION
0
2
4
6
8
10
12
14
16
$M_{\mu\bar{\mu}}$ (GeV)

Fig. 21

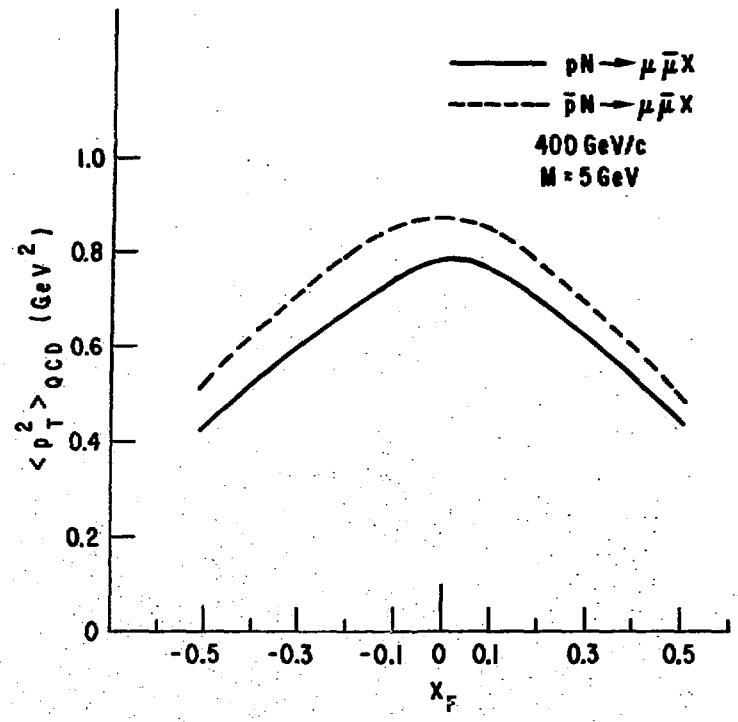
pN → μμ̄X
p̄N → μμ̄X
400 GeV/c
M = 5 GeV
1.0
0.8
0.6
0.4
0.2
0
$\langle p_T^2 \rangle_{QCD}$ (GeV^2)
-0.5
-0.3
-0.1
0
0.1
0.3
0.5
X_F

Fig. 22